Postprint: Kamp, J.; Kraume, M. (2016), From single drop coalescence to droplet swarms – Scale-up considering the influence of collision velocity and drop size on coalescence probability, Chemical Engineering Science, 156, 162–177, https://doi.org/10.1016/j.ces.2016.08.028

From single drop coalescence to droplet swarms – Scale-up considering the influence of collision velocity and drop size on coalescence probability

Johannes Kamp*, Matthias Kraume
Chair of Chemical & Process Engineering, Technische Universität Berlin,
Straße des 17. Juni 135, FH 6-1, 10623 Berlin, Germany
*Corresponding author: Johannes.Kamp@tu-berlin.de Tel.: +49 30 314 23171

Coalescence modelling in liquid/liquid dispersions is a challenging task and field of investigations up to now, which becomes apparent when comparing the various existent models with their different and partly even contradictive implementation of influencing factors. In this work, systematic investigations of single drop coalescence were used to compare and validate different coalescence efficiency models regarding the important influencing parameters relative collision velocity and drop size. The impact of these parameters could be analysed independently from each other for the first time and used to identify the best modelling approach. Moreover, the numerical parameter of the coalescence efficiency model could be obtained based on single drop experiments. Using this determined parameter the simulation of drop size distributions within a lab scale stirred vessel was possible. The presented method offers the possibility of independent parameter estimation for population balance equation simulations based on single drop experiments. The application of this systematic approach allows the separate validation of submodels and reliable parameter determination by small scale investigations. On this basis a sound scale-up is possible using population balance equation simulations.

Keywords: coalescence, coalescence efficiency, population balance equation, model validation, collision velocity, drop size

1. Introduction

In many technical applications liquid/liquid systems are an integral part of a production process, i.e. in extraction columns or stirred tanks. The drop size distribution within these apparatuses is formed by drop breakage and coalescence and determines the overall efficiency of the process. Hence, a similar drop size distribution is the main goal for scale-up from lab scale to production scale. However, empirical scale-up rules are used up to now which require geometric similarity and constant impeller tip speed or power input (Ghotli et al., 2013). Apart from that, a mechanistic approach using population balance equations (PBE) (Liao and Lucas, 2010, 2009) was established in the past years using single drop investigations to describe the fundamental phenomena breakage and coalescence in PBE (Bart et al., 2006; Kamp and Kraume, 2015; Kopriwa et al., 2012; Maaß and Kraume, 2012; Villwock et al., 2014b). Using PBE, which describe the breakage and coalescence rate by separate submodels, a bottom-up approach from small scale single drop experiments to droplet swarms in technical applications can be performed directly omitting empirical scale-up and pilot plant scale investigations. As drop breakage was investigated in detail by several authors (Ghotli et al., 2013; Lasheras et al., 2002; Maaß, 2011; Maaß et al., 2011a; Solsvik et al., 2013) and the bottom-up approach was applied successfully focussing on

the drop breakage (Maaß and Kraume, 2012), this work focusses on drop coalescence and its modelling in PBE.

1.1. Drop Coalescence

Coalescence describes the confluence of two disperse droplets or a drop with the corresponding continuous phase. Before coalescence between two droplets occurs, the interfaces approach each other and a thin film of surrounding continuous phase has to drain between the interfaces. At a certain critical distance the continuous phase film ruptures and the drops confluence. However, a collision of droplets does not end in coalescence necessarily, but may also results in a repulsion or agglomeration of the droplets. The probability of coalescence after droplet collision is described by the coalescence efficiency in PBE. The coalescence efficiency is influenced by numerous factors especially surface active components in already small amounts (Kamp et al., 2016b). Due to the involved complex interactions in distances of several orders of magnitude, numerous modelling approaches can be found in literature (Liao and Lucas, 2010) which implement influencing factors differently and in parts even contradictorily (Kamp et al., 2016b; Kopriwa et al., 2012).

1.2. Drop rise velocity and surface mobility

To determine the purity of a system and the interface of investigated droplets in particular, the drop rise velocity is a very sensitive parameter. Already small changes at the interface result in an altered surface mobility and, thus, increased friction coefficient which again diminishes the rise velocity (Villwock et al., 2014a; Wegener et al., 2014). A force balance of a single drop with diameter d_p leads to the terminal drop rise velocity:

$$v_t = \sqrt{\frac{4}{3}\frac{|\varrho_d - \varrho_c|}{\varrho_c}\frac{g d_p}{C_D}} \tag{1}$$

with disperse ϱ_d and continuous density ϱ_C, gravitational acceleration g and drag coefficient C_D. Considering inertia force additionally, the transient drop rise velocity of a fluid particle becomes:

$$\frac{\mathrm{d}v_p}{\mathrm{d}t} = \frac{|\varrho_c - \varrho_d|}{\varrho_d + \alpha\varrho_c} g - \frac{3}{4} C_D \frac{\varrho_c}{\varrho_d + \alpha\varrho_c}\frac{v_p^2}{d_p} \tag{2}$$

using the coefficient α accounting for the virtual mass of continuous phase which is accelerated with the droplet (Wegener et al., 2014, 2007). To calculate the drag coefficient C_D several correlations are available (Wegener et al., 2014), in this work the correlation of Feng and Michaelides (2001) for a viscosity ratio $0 \leq \mu^* = \frac{\mu_d}{\mu_c} \leq 2$ was used:

$$C_D = \frac{2-\mu^*}{2}\frac{48}{Re}\left(1 + \frac{2.21}{\sqrt{Re}} - \frac{2.14}{Re}\right) + \frac{4\mu^*}{6+\mu^*} 17 Re^{-\frac{2}{3}} \tag{3}$$

with Reynolds number

$$Re = \frac{v_p d_p \varrho_c}{\mu_c}. \tag{4}$$

Wegener et al. (2010) found that the model of Feng and Michaelides (2001) describes the rise velocity of toluene drops with fully mobile interface reasonably well. Additionally, this drag coefficient correlation is the only one which predicts reliable values for Reynolds numbers above 100 (Wegener et al., 2014) which occurred in the investigations.

1.3. Population Balance Equation (PBE)

The PBE balances the convective flows $f_i \cdot \dot{V}_i$ over the regarded volume boundaries and describes the time dependent number density distribution $f(d_p, t)$ of particles / drops with diameter d_p by positive (birth) and negative (death) source terms for droplet breakage and coalescence respectively (Hulburt and Katz, 1964; Kopriwa et al., 2012; Ramkrishna, 2000; Randolph and Larson, 1962; Sporleder et al., 2012). These terms are given by mechanistic submodels: the number of daughter droplets $n_d(d_p)$, daughter drop size distribution $\beta(d_p, d_p')$, breakage rate $g(d_p)$ including two numerical parameters (termed in this work: $c_{1,b}$ and $c_{2,b}$), collision frequency $\xi(d_p, d_p')$ with one numerical parameter ($c_{1,c}$) and coalescence efficiency $\lambda(d_p, d_p')$ with the numerical parameter $c_{2,c}$ (Liao and Lucas, 2010, 2009). The volume-related PBE for liquid/liquid dispersions without convective flows becomes (Attarakih et al., 2004; Gäbler et al., 2006; Liao and Lucas, 2010; Valentas and Amundson, 1966):

$$\begin{aligned}\frac{\partial f(d_p,t)}{\partial t} = &\int_{d_p}^{d_{p,max}} n_d(d_p') \cdot \beta(d_p, d_p') \cdot g(d_p') \cdot f(d_p', t)\,\mathrm{d}d_p' - g(d_p) \cdot f(d_p, t) \\ &+ \frac{1}{2}\int_0^{d_p} \xi(d_p'', d_p') \cdot \lambda(d_p'', d_p') \cdot f(d_p', t) \cdot f(d_p'', t)\,\mathrm{d}d_p' \\ &- f(d_p, t) \cdot \int_0^{d_{p,max}-d_p} \xi(d_p, d_p') \cdot \lambda(d_p, d_p') \cdot f(d_p', t)\,\mathrm{d}d_p'\end{aligned} \tag{5}$$

using the definition $d_p'' = \left(d_p^3 - {d_p'}^3\right)^{1/3}$.

The submodels for breakage and coalescence used in this work are summarised in Table 1. The most widely used PBE model for turbulent liquid/liquid dispersions is the film drainage model of Coulaloglou and Tavlarides (1977). The authors introduced a phenomenological breakage rate $g(d_p)$ by multiplying the reciprocal time needed for the drop breakup to occur ($t_{breakup}$) and the fraction of breaking drops which resulted in Equation (10) (see Table 1). A multitude of different breakage rate submodels were developed in the past decades (Liao and Lucas, 2009). In this study only one other breakage rate model is used: the submodel of Chen et al. (1998) considers drop viscoelasticity in addition to the Coulaloglou and Tavlarides (1977) model. Moreover, Chen et al. (1998) criticised the maximum of Coulaloglou and Tavlarides' (1977) breakage rate to be physically not realistic. Thus, Chen et al. (1998) assumed the breakage time to be constant and obtain a strictly increasing breakage rate (Equation (11) in Table 1).

The coalescence rate is composed of collision frequency $\xi(d_p, d_p')$ and coalescence probability (or efficiency) $\lambda(d_p, d_p')$:

$$F(d_p, d_p') = \xi(d_p, d_p') \cdot \lambda(d_p, d_p')\,. \tag{6}$$

The collision frequency of Coulaloglou and Tavlarides (1977) $\xi_{C\&T}(d_p, d_p')$ (Equation (13) in Table 1) was derived from the kinetic theory of gases assuming that collisions of drops in a locally isotropic turbulent flow are analogous to interactions of molecules. As other collision frequency submodels for turbulent collisions are comparable (Liao and Lucas, 2010) only the submodel $\xi_{C\&T}$ of Coulaloglou and Tavlarides (1977) is used in this study.

Concerning the coalescence efficiency $\lambda(d_p, d_p')$, on which this work is focussed, Coulaloglou and Tavlarides (1977) related the film drainage time to the contact time of two colliding droplets.

This general mechanistic approach is commonly termed film drainage model. They postulated that the drops must stay in contact longer than the film drains down to the critical film rupture distance and obtained Equation (14) (see Table 1). The factor $(1+\varphi)^{-3}$ was introduced to account for "damping" effects on the local turbulent intensities at high hold-up fractions.

Other film drainage models used in this study are the ones proposed by Prince and Blanch (1990) and Henschke et al. (2002). The formulation of the Prince and Blanch (1990) model by Equation (15) in Table 1 was obtained by merging all constants into the numerical parameter $c_{2,c}$. Additionally, the characteristic length of turbulent interactions of two drops was assumed to be $d_p + d'_p$ according to Coulaloglou and Tavlarides (1977), resulting in the contact time:

$$t_{contact} = \frac{\left(d_p+d'_p\right)^{2/3}}{\epsilon^{1/3}}. \tag{7}$$

Under these assumptions the Prince and Blanch (1990) model is identical to the coalescence efficiency of Chesters (1991) assuming turbulence induced coalescence and fully mobile interfaces.

Henschke et al. (2002) developed an asymmetrical film drainage model to describe the drainage time in horizontal separators. Kopriwa (2014) derived the corresponding coalescence efficiency (Equation (16) in Table 1) by relating the drainage time of Henschke et al. (2002) to the contact time in turbulent flow according to Equation (7). The Hamaker constant was assumed by Henschke et al. (2002) to be $A_{1,2,3} = 10^{-20}$ Nm for oil/water systems. All constant and fitting parameters were merged into $c_{2,c}$ in Equation (16).

Apart from several variations of the film drainage model (Liao and Lucas, 2010) other modelling approaches were developed: the energy model and the critical approach velocity model.

The energy model (Equation (17) in Table 1) was developed by Sovova (1981) based on Howarth's (1964) assumptions and relates the kinetic energy of the approaching droplets to their surface energy. Thus, the model assumes that for coalescence the surface energy has to be exceeded by the kinetic energy. However, Sovova (1981) combined it with the film drainage model but Simon (2004) proposed to use it solely. Originated in the model assumptions, the film drainage models and the energy model describe the influence of the energy dissipation rate contrarily: $\lambda_{\mathrm{C\&T}} \propto \exp(-\epsilon)$, $\lambda_{\mathrm{P\&B}}, \lambda_{Hen} \propto \exp\left(-\epsilon^{1/3}\right)$ and $\lambda_{Sov} \propto \exp\left(-\epsilon^{-2/3}\right)$.

For a locally isotropic and homogeneous turbulence the energy dissipation rate ϵ can be correlated to the relative velocity of two droplets moving in an eddy of the size $d_p + d'_p$ (Coulaloglou and Tavlarides, 1977; Hinze, 1955; Kolmogorov, 1941):

$$v_{rel} = \sqrt{2}\left(\epsilon\left(d_p + d'_p\right)\right)^{1/3}, \tag{8}$$

which is commonly assumed to equal the collision velocity of the drops. Although, the flow in actual applications may not satisfy the condition of Kolmogorov's theory assuming locally isotropic and homogeneous turbulence, it is most widely used to approximate turbulence and allow a simple description of the system. All presented models use this assumption which is technically speaking only valid in the inertial subrange of turbulence (Frisch, 1995; Solsvik and Jakobsen, 2016).

The critical approach velocity model was proposed by Lehr and Mewes (2001). It assumes the relative velocity being the main influencing parameter of droplet coalescence and postulates a critical velocity above which coalescence is hindered. Due to inconsistencies the original model equation was corrected by Liao and Lucas (2010) to Equation (18) (see Table 1).

In the case that the critical approach velocity is determined experimentally (Lehr et al., 2002), the coalescence efficiency only depends on the relative velocity. However, the critical approach velocity model is as well contradictory to the energy model.

In several modelling approaches of coalescence the equivalent drop diameter d_{eq} is used to consider the collision of unequally sized drops with diameter d_p and d'_p :

$$d_{eq} = \frac{2 d_p d'_p}{d_p + d'_p}, \tag{9}$$

which can be deduced from Young-Laplace equation (Butt et al., 2003; Princen, 1969).

Table 1: Used breakage and coalescence submodels of PBE in this work

Breakage rate $g(d_p)$		
Coulaloglou & Tavlarides (1977)	$g_{C\&T} = c_{1,b} \frac{\epsilon^{1/3}}{(1+\varphi) d_p^{2/3}} \cdot \exp\left(-c_{2,b} \frac{\gamma (1+\varphi)^2}{\varrho_d \epsilon^{2/3} d_p^{5/3}}\right)$	(10)
Chen et al. (1998)	$g_{Chen} = c_{1,b} \cdot \exp\left(-c_{2,b} \frac{\gamma (1+\varphi)^2}{\varrho_d \epsilon^{2/3} d_p^{5/3}} - c_{3,b} \frac{\mu_d (1+\varphi)}{\varrho_d \epsilon^{1/3} d_p^{4/3}}\right)$	(11)
Daughter drop size distribution $\beta(d_p, d'_p)$		
Coulaloglou & Tavlarides (1977)	$\beta_{C\&T}(V_p,\ V'_p) = \frac{1}{V_\sigma \sqrt{2\pi}} \exp\left(-\frac{(V_p - V_\mu)^2}{2 V_\sigma^2}\right)$ with: $V_\sigma = \frac{V'_p}{c_\beta n_d},\ V_\mu = \frac{V'_p}{n_d},\ V_p = \frac{\pi}{6} d_p,\ n_d = 2$	(12)
Collision frequency $\xi(d_p,\ d'_p)$		
Coulaloglou & Tavlarides (1977)	$\xi_{C\&T} = c_{1,c} \frac{\epsilon^{1/3}}{1+\varphi} \left(d_p + d'_p\right)^2 \left(d_p^{2/3} + d_p'^{\,2/3}\right)^{1/2}$	(13)
Coalescence efficiency $\lambda(d_p,\ d'_p)$		
Film drainage models		
Coulaloglou & Tavlarides (1977)	$\lambda_{C\&T} = \exp\left(-c_{2,c} \frac{\mu_c \varrho_c \epsilon}{\gamma^2 (1+\varphi)^3} \left(\frac{d_p d'_p}{d_p + d'_p}\right)^4\right)$	(14)
Prince & Blanch (1990)	$\lambda_{P\&B} = \exp\left(-c_{2,c} \frac{\varrho_c^{1/2} \epsilon^{1/3}}{\gamma^{1/2}} \frac{\left(d_p d'_p\right)^{3/2}}{\left(d_p + d'_p\right)^{13/6}}\right)$	(15)
Henschke et al. (2002) according to Kopriwa (2014)	$\lambda_{Hen} = \exp\left(-c_{2,c} \frac{\mu_c \epsilon^{1/3}}{A_{1,2,3}^{1/6} \gamma^{1/3} \left(\lvert \varrho_d - \varrho_c \rvert g\right)^{1/2}} \frac{\left(d_p d'_p\right)^{1/3}}{\left(d_p + d'_p\right)}\right)$	(16)
Energy model		
Sovova (1981) according to Simon (2004)	$\lambda_{Sov} = \exp\left(-c_{2,c} \frac{\gamma}{\varrho_d \epsilon^{2/3}} \frac{(d_p^2 + d_p'^2)(d_p^3 + d_p'^3)}{d_p^3 d_p'^3 \left(d_p^{2/3} + d_p'^{2/3}\right)}\right)$	(17)
Critical approach velocity (CAV) model		
Lehr & Mewes (2001) according to Liao & Lucas (2010)	$\lambda_{L\&M} = \min\left(\frac{v_{crit}}{v_{rel}}, 1\right)$ with $v_{crit} = \sqrt{\frac{0.06\,\gamma\,(d_p + d'_p)}{2\,\varrho_c\,d_p\,d'_p}}$	(18)

Up to now, the PBE submodels are fitted to droplet swarm experiments in which a complex superposition of drop breakage and coalescence exists and the respective influences on the drop size distribution cannot be distinguished. Considering the five presented modelling approaches of coalescence efficiency it becomes apparent that the mechanisms of droplet coalescence are still not fully understood. The dissimilar and partly contradictive model dependencies on drop diameter and energy dissipation rate were discussed for additional models by Kopriwa et al. (2012) and Kamp et al. (2016b). Hence, fundamental investigations are necessary to validate the existent models and develop more accurate ones. Therefore, in this study single drop experiments were performed in a coalescence cell (Kamp and Kraume, 2014). The obtained results were used to validate the coalescence models concerning the influence of drop diameter and relative velocity separately. Subsequently, the results were transferred to drop swarm simulations in a stirred tank and compared to experimental drop size distributions.

2. Materials and methods

2.1. Experimental set-up

The investigated liquid phases were toluene (disperse) and water (continuous) for both single drop and droplet swarm experiments. This system is one of the EFCE standard test systems for extraction (Misek et al., 1985) and, thus, provides comparability and transferability to other physical systems. The measured physical quantities of the liquid phases are given in Table 2. Due to the high purity requirements only chemicals with analysis grade were used and all equipment with contact to the liquid phases was made of glass, stainless steel or PTFE. To avoid contaminations the equipment was cleaned thoroughly and rinsed with deionised water extensively prior to use.

Table 2: Physical quantities of the liquids at $\vartheta = 25°C$

Water			Toluene	
Density ϱ_c	Viscosity μ_c	Interfacial tension γ	Density ϱ_d	Viscosity μ_d
997 kg/m^3	$8.84 \cdot 10^{-4}$ Pa · s	$35 \cdot 10^{-3}$ N/m	862 kg/m^3	$5.41 \cdot 10^{-4}$ Pa · s

Single drop coalescence test cell

The investigated liquid phases were toluene p.a. (Merck 1.08325.2500) and ultrapure water with a resistivity of 18.3 MΩ · cm produced by the purification systems Werner EASYpure UV or Elga Purelab flex 2. All experiments were conducted at a temperature of $\vartheta = 24.5 \pm 0.5$ °C. To avoid undesired mass transfer between toluene and water due to a slight mutual miscibility, the phases were saturated with each other in a separatory funnel.

For the single drop experiments the automated coalescence test cell of Kamp and Kraume (2014) was used in which a collision of a rising droplet with a pendant one is induced within a quiescent continuous phase. The test cell of about 0.5 L volume has quartz glass walls in front and back to provide optical accessibility. Within the test cell the droplets are produced by syringe pumps at the tips of two vertical cannulas opposing each other. The oil drop at the lower cannula detaches, accelerates, rises through the continuous water phase and collides with the upper pending drop. The drop sizes and distance can be varied which also influences the drop

rise and collision velocity. The droplet rise and collision was recorded by a CMOS high speed camera with LED backlight. Two different high speed cameras were used:

(1) Photonfocus MV-D752-160-CL-8 (maximum resolution of 752 × 582 pixels at a frame rate of 350 fps) with frame grabber board Silicon Software microenable III, Pentax TV lens 12 mm and synchronised LED flash CCS LDL-TP-100/100-R,
(2) VisionResearch Phantom v711 monochrome (maximum resolution of 1280 x 800 pixels at a frame rate of 7530 fps) with Sigma APO macro lens 180 mm F2.8 EX DG OS HSM and continuous LED backlight GS Vitec MultiLED LT-V8-15.

Detailed information about set-up and experimental procedure can be found in Kamp and Kraume (2014). The drop sizes of the rising drop d_{bot} and the pendant drop d_{top} were both varied between 1.5 mm $\leq d_{bot/top} \leq$ 2.9 mm and the drop distance between 0.5 mm $\leq h \leq$ 17 mm.
In order to prove the purity of the investigated system, the rising path of the lower droplet was analysed according to the procedure described in Villwock et al. (2014a). As already small impurities affect the surface mobility of a drop and, thus, increase the drag coefficient, the terminal rise velocity is a very sensitive parameter. The investigated rise trajectory was compared to trajectories obtained by empirical correlations. Experiments were only performed if the experimental drop rise velocity agreed with the theoretical velocity of a drop with fully mobile interface (see also section 3.1).
The recorded images were analysed using the Matlab ® Image Processing Toolbox. After background removal and threshold setting the droplets were identified and the centroids of the drops were detected for every frame. By combining the data of all frames of one recorded sequence the trajectory of the lower drop was determined. The trajectories of all sequences with identical parameter settings were averaged and used for further analysis. In case of the fully automated high speed camera set-up (1) at least 100 drop collisions were averaged for every data point. As high speed camera set-up (2) had to be triggered manually only about 20 drop collision events were evaluated due to the higher experimental efforts. Detailed information about the applied automated image analysis and post-processing can be found in Kamp et al. (2016a).

Stirred tank

The droplet swarm experiments were performed in a baffled stirred tank DN 150 ($H_t/D_t = 1$) equipped with a Rushton turbine ($d_i/D_t = 0.33$, $h_i/H_t = 0.33$) at a temperature of $\vartheta = 20$ °C. The drop size distribution was obtained by an endoscope technique in the stirred tank and a subsequent manual image analysis. For detailed description of this set-up and endoscope technique see Maaß et al. (2011b) and Ritter and Kraume (2000).
The examined disperse phase was toluene p.a. (Merck 1.08325.2500) and continuous phase was deionised water with pH set to 7 by addition of potassium hydroxide (Merck 1.09921.0001). The total volume in the vessel was $V_t = 2.58$ L with a volumetric phase fraction of disperse phase $\varphi = 0.1$. Three stirrer frequencies ($n = 400, 550, 700\ \mathrm{min}^{-1}$) were investigated which yield Reynolds numbers in the tank of $\mathrm{Re_t} = n^2 d_i \varrho_{disp}/\mu_{disp} > 2 \cdot 10^9$. The corresponding mean energy dissipation rates in the stirred tank $\epsilon = 0.133, 0.345, 0.712\ \mathrm{m^2/s^3}$ were calculated using the impeller's power number $Ne = 3.8$ in a fully turbulent flow regime ($\mathrm{Re} > 10^4$): $\epsilon = {}^{P}/_{M} = Ne\, n^3 d_i^5/V_t$. The drop size distributions were measured at distinct times after starting the impeller.

2.2. Simulations

The simulations of the stirred tank were performed in this study by an integral single zone PBE (Equation 5) of the whole batch reactor with a mean energy input ϵ generated by the impeller. The basic model implementation was done with the Coulaloglou and Tavlarides (1977) submodels for drop breakage and coalescence. To avoid a violation of conservation of mass due to numerical loss of mass, a narrower normal daughter drop size distribution $\beta(d_p, d_p')$ than proposed by Coulaloglou and Tavlarides (1977) was used (see Equation (12) in Table 1) using a standard deviation tolerance of $c_\beta = 5$ (instead of 3) within V_σ. According to Coulaloglou and Tavlarides (1977) binary drop breakup was assumed ($n_d = 2$) (Kamp and Kraume, 2015).
In some parts of this work other submodels for breakage rate and coalescence efficiency were applied (see section 1.3). In that case, the model modification was indicated and discussed explicitly at this point.
It was found that variations of the initial drop size distribution had only minor influence on the simulation results within the first milliseconds of the simulations. Hence, a Gaussian initial drop size distribution with mean value $d_\mu = 1$ mm and standard deviation $d_\sigma = 50$ µm was used arbitrarily (Kamp and Kraume, 2015).
All variables and parameters are given in SI units if dimensional; $c_{2,c}$ of the Coulaloglou and Tavlarides (1977) model has the dimension [m^{-2}]. The geometric data, energy dissipation rates and phase fraction were implemented according to the experimental set-up described above. The physical quantities used are given in Table 2.

To solve the partial differential equation of the PBE with coupled mass balance the commercial software PARSIVAL® (Wulkow et al., 2001) was used. The implemented parameter estimation routine of PARSIVAL® was used to fit the numerical parameters of breakage and coalescence rate of the different models by minimising the residual between experimental and simulated data. In this work the root-mean-square deviation (RMSD) was used to quantify differences between n experimental values X_i and simulation results $\hat{X}_i$:

$$\mathrm{RMSD}(X) = \sqrt{\frac{\sum_{i=1}^{n}(X_i - \hat{X}_i)^2}{n}}. \qquad (19)$$

3. Results and discussion

In this work systematic investigations of single drop coalescence were used to compare and evaluate different coalescence efficiency models regarding the influencing parameters relative collision velocity and drop size. Based on these results valid coalescence efficiency models were identified and drop size distributions in a stirred tank were simulated.
First the validity and reproducibility of single drop experiments by analysis of droplet rise velocity is discussed. On this basis, the coalescence probabilities of two colliding drops were investigated systematically varying droplet sizes and collision velocity. With these results the different modelling approaches from literature were compared and evaluated. Moreover, restrictions of experiments and models are discussed. The coalescence efficiency submodels were fitted to the single drop data concerning drop size and collision velocity. The best model with the obtained fitting parameter was then used to perform a scale-up from these single drop investigations to a stirred tank. Using PBE the drop size distribution was simulated with the fitted Coulaloglou and

Tavlarides (1977) film drainage model and compared to experimental distributions in a stirred tank DN 150.

3.1. Drop rise velocity

As the drop rise velocity is a very sensitive quantity concerning the purity of drop interface (Villwock et al., 2014a; Wegener et al., 2014), the drop trajectory was recorded and analysed prior every experiment to ensure that no impurities were existent in the coalescence test cell. In order to establish a reference for these purity tests, the trajectories for different rising drop sizes were investigated with serious effort to avoid contaminations. For every drop size at least 100 trajectories were recorded and analysed. These were compared to theoretical trajectories calculated using the drag coefficient correlation of Feng and Michaelides (2001) (Equation (3)). Even though the correlation was developed to calculate the steady-state drag coefficient, it can also be used to describe the transient droplet trajectory quite well (Wegener et al., 2014). By regarding the trajectory being one-dimensional in height h direction Equation (2) can be transformed to a spatial-dependent form:

$$\frac{\mathrm{d}v_p}{\mathrm{d}h} v_p = \frac{|\varrho_c - \varrho_d|}{\varrho_d + \alpha \varrho_c} g - \frac{3}{4} C_D \frac{\varrho_c}{\varrho_d + \alpha \varrho_c} \frac{v_p^2}{d_p} . \qquad (20)$$

The virtual mass coefficient was set to $\alpha = 0.75$ according to Wegener et al. (2007) and Equation (20) was solved using Matlab® *ode45* solver starting with an initial velocity of $v_0 = 10^{-6}$ m/s at $h_0 = 0$ mm. The obtained experimental trajectories (including the standard deviation) and calculated rising paths are shown in Figure 1.

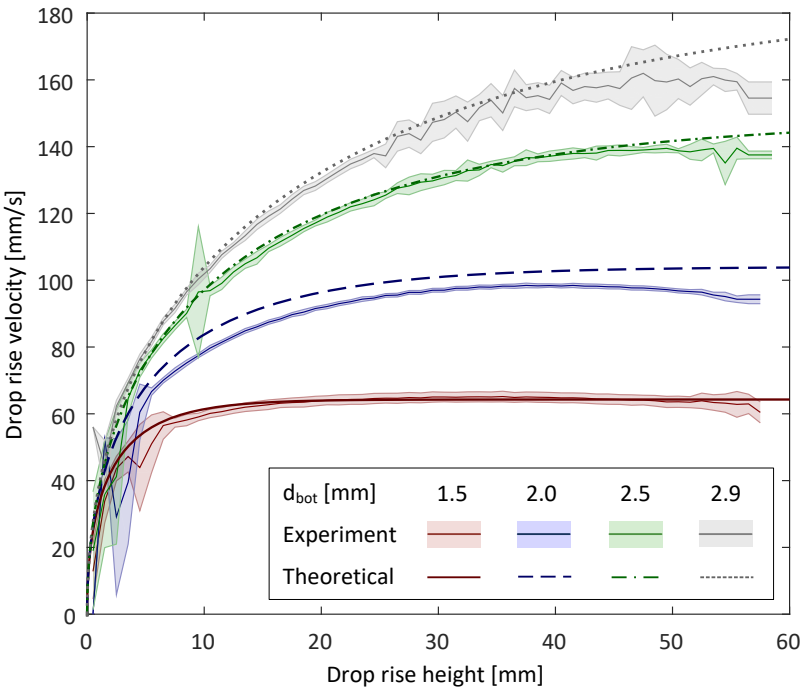

Figure 1: Drop rise velocity over rise height of different drop sizes in experiments (mean values and standard deviations) and calculations using the drag coefficient correlation of Feng and Michaelides (2001).

The mean curves of the experimental trajectories were obtained by analysing at least 100 sequences per drop size. From the rise heights of the single drops the corresponding minimal, maximal and mean velocities as well as standard deviations were calculated (Kamp et al., 2016a). At rise heights >45 mm the droplets approached the border of optical lens which focused the rays of light to the CMOS image sensor. From this point optical aberrations let the drops seem to decelerate again in Figure 1. In fact, a constant terminal drop rise velocity was achieved. Fluctuations and higher standard deviations of the rise velocity during the first millimetres of rising are caused by the drop detachment from the lower cannula. The sessile oil drops at the lower cannula are detached by a short pulse of water through the cannula to break the adhesion of the droplet at the cannula's rim (see details in Kamp and Kraume (2014)). Due to the tearing off from the cannula, oscillations of the drop surface are induced which diminish during the first millimetres of rising.

The comparison between the experimental data and the calculated trajectory (Equation (20)) and terminal rise velocity (Equation (1)) shows good consistence for drop sizes of $d_p = 1.5, 2.5, 2.9$ mm. Only the drop rise velocity of drop size $d_p = 2.0$ mm lies below the theoretical graph. The corresponding theoretical terminal drop rise velocity is 104 mm/s but the experimentally observed terminal velocity was 99 mm/s. This is an example for a slightly contaminated system in which the surface mobility is reduced due to adsorbed surfactants and, thus, the rise velocity diminishes. The complete coverage with surfactants (resulting in the drag coefficient of a rigid sphere) would result in a terminal rise velocity of 63 mm/s (determined by the drag coefficient correlation of Brauer and Mewes (1972)). Comparing these values it can be concluded that the contamination is small but observable.

For the biggest drop ($d_p = 2.9$ mm) a significant increase of the standard deviation was observed for rise heights >25 mm. This occurs due to the fact that the droplets are big enough to change to the oscillatory regime. The drop oscillations cause a variation of the rise velocity and reduce the mean velocity below the theoretical terminal rise velocity of a spherical droplet. The used correlation of Feng and Michaelides (2001) was derived for spherical drops which explains the deviations to the experiments.

In conclusion, the theoretical drop rise velocities using the drag coefficient correlation of Feng and Michaelides (2001) (Equation (3)) were found to correspond to experimentally investigated drop trajectories in a non-contaminated system. By comparing the theoretical and experimental rise velocity it can be tested if the drops have a fully mobile surface and, thus, if the system is free of surfactants. With this method undesired contaminations which influence the coalescence probability can be detected prior to experimental runs.

With the knowledge of the droplet's trajectory, a drop collision with a defined velocity can be obtained by positioning a pendant drop into the rising path of the lower droplet at the corresponding height during acceleration period. The successful application of this method is shown in Figure 2. Three mean trajectories of a rising droplet of $d_{bot} = 2.5$ mm are plotted varying the collision height with the pendant drop. The trajectories are nearly identical and overlay each other. Only at the beginning an increased standard deviation of the drop rise velocity occurs due to the mentioned oscillations caused by drop detachment. The pendant drop has no significant influence on the rise velocity and induces a deceleration only few tens of a millimetre before collision. The collision (or "contact") of the droplets is defined here as the distance at which the undeformed droplets would touch each other, thus the point where their centres of mass have a separation distance equal to the sum of their radii:

$$s_{collison} = \frac{1}{2}(d_1 + d_2)\,. \qquad (21)$$

In optical observations the moment of collision corresponds (with sufficient accuracy) to the recorded frame at which the drop's borders overlap each other visually.

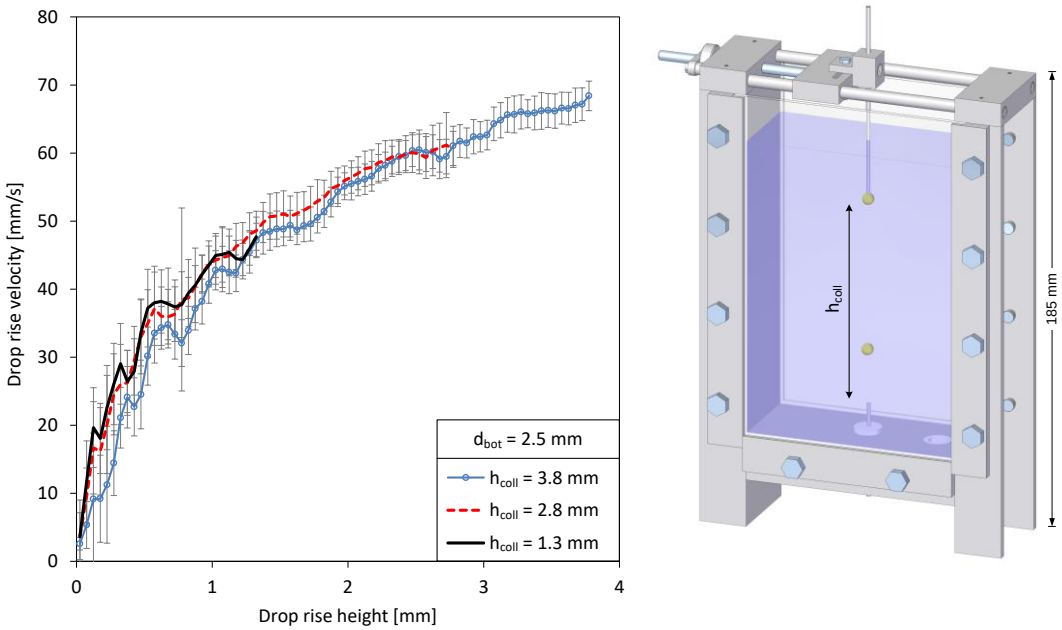

Figure 2: Drop rise velocity for different rise heights (left) and variation of drop rise height in the test cell to adjust collision velocities (right).

The successful adjustment of drop sizes and relative collision velocity independently from another offered the possibility of a systematic analysis of these influencing factors which is described in the following.

3.2. Single drop investigations & model validation

It has to be mentioned here that investigating the coalescence probability is not a trivial task as the result is highly sensitive to numerous influencing factors which cannot be analysed separately in all cases. Earlier investigations showed that the influences of drop diameter and collision velocity on the coalescence efficiency superimpose each other with collision velocity having a greater influence compared to the drop diameter (Kamp and Kraume, 2014). Furthermore, drop oscillations were identified to have significant impact on coalescence probability in single drop investigation of Scheele and Leng (1971). These influencing parameters are discussed in this section trying to identify their impact on the coalescence probability, respectively. Additionally, the results are compared with the (partly contradictory) coalescence efficiency models introduced in Table 1 to analyse their validity.

Relative collision velocity

As the collision velocity v_{coll} was found to have greater impact on coalescence efficiency this parameter is discussed first. In Figure 3 the coalescence efficiency is shown against the mean relative collision velocities for all drop sizes investigated (1.5 mm $\leq d_{bot/top} \leq$ 2.9 mm). Black circles in Figure 3 indicate experiments with fully automated high speed camera set-up (1) and

at least 100 drop collisions were recorded for every data point. Grey circles show data obtained with manually triggered high speed camera set-up (2). The gained pictures have higher quality but experiments and analysis were more time consuming so that only about 20 drop collisions were recorded per data point. With camera set-up (2) higher temporal resolutions of the coalescence process could be achieved which allowed the investigation of drop deformations during collision and determination of contact and coalescence times (data not shown). No deviations which depend on the type of set-up were observed for identical experimental parameters.
As can be clearly seen, no coalescence could be observed for collision velocities above $v_{max} = 60$ mm/s. For velocities $v_{coll} < v_{max}$ the coalescence efficiency scatters from 0 to 1 which can be attributed to the influence of other parameters such as the droplet size and oscillation which are discussed later. Velocities below 20 mm/s could not be achieved experimentally within the given boundaries as this would require drop distances below 0.5 mm or significantly smaller drop sizes.

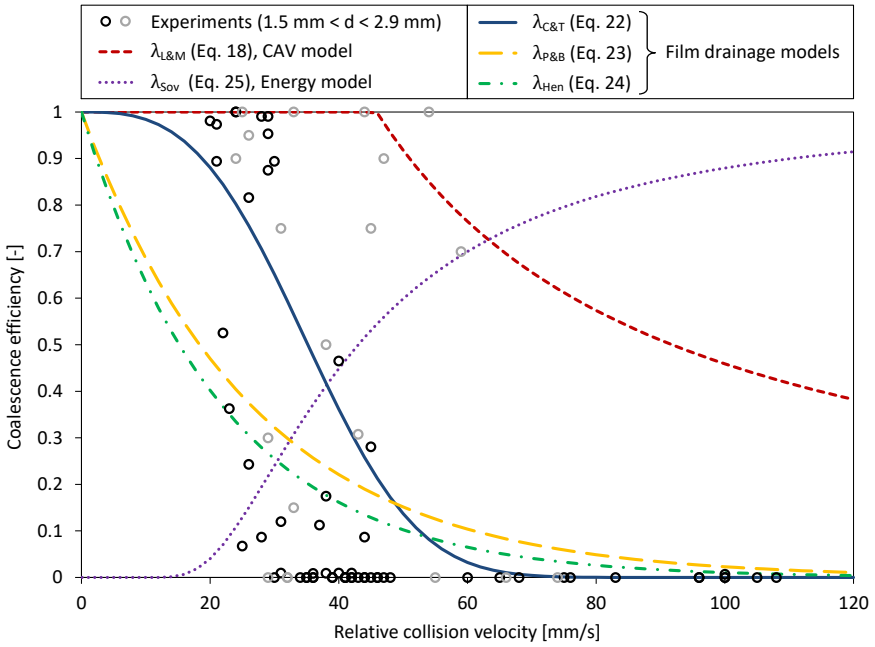

Figure 3: Dependency of coalescence efficiency on relative collision velocity for all investigated drop sizes (1.5 mm $< d_{top}, d_{bot} <$ 2.9 mm) and the models of Coulaloglou and Tavlarides (1977), Prince and Blanch (1990), Henschke et al. (2002), Lehr and Mewes (2001) and Sovova (1981) using a constant drop size $d_p = d'_p = 1$ mm. Experiments represented by black circles were achieved using high speed camera set-up (1) and by grey circles using high speed camera set-up (2).

To analyse the velocity dependency of the coalescence efficiency models, the energy dissipation rate was replaced by the relative velocity with the above discussed correlation (Equation (8)). The resulting coalescence efficiency models are given in Table 3. The dampening factor $(1 + \varphi)^{-3}$ of disperse phase within the Coulaloglou and Tavlarides (1977) model was neglected for the single drop experiments.

Table 3: Dependency of coalescence efficiency models on relative collision velocity obtained by replacing the energy disspation rate using Equation (8).

Reference	**Coalescence efficiency $\lambda(v_{rel})$**	
Coulaloglou & Tavlarides (1977) with $c_{2,c} = 2 \cdot 10^{12}$ m^{-2}	$\lambda_{C\&T} = \exp\left(-c_{2,c}\frac{\mu_c \varrho_c v_{rel}^3}{\gamma^2 \sqrt{8}(d_p + d_p')}\left(\frac{d_p\, d_p'}{d_p + d_p'}\right)^4\right)$	(22)
Prince & Blanch (1990) with $c_{2,c} = 20$	$\lambda_{P\&B} = \exp\left(-\frac{c_{2,c}}{\sqrt{2}}\frac{\varrho_c^{1/2} v_{rel}}{\gamma^{1/2}}\frac{\left(d_p\, d_p'\right)^{3/2}}{\left(d_p + d_p'\right)^{5/2}}\right)$	(23)
Henschke et al. (2002) with $c_{2,c} = 10$	$\lambda_{Hen} = \exp\left(-\frac{c_{2,c}}{\sqrt{2}}\frac{\mu_c v_{rel}}{A_{1,2,3}^{1/6}\gamma^{1/3}\left(\lvert\varrho_d - \varrho_c\rvert g\right)^{1/2}}\frac{\left(d_p\, d_p'\right)^{1/3}}{\left(d_p + d_p'\right)^{4/3}}\right)$	(24)
Sovova (1981) with $c_{2,c} = 5 \cdot 10^{-3}$	$\lambda_{Sov} = \exp\left(-c_{2,c}\frac{2\gamma\left(d_p^2 + d_p'^2\right)\left(d_p^3 + d_p'^3\right)\left(d_p + d_p'\right)^{2/3}}{\varrho_d\, v_{rel}^2\, d_p^3\, d_p'^3\left(d_p^{2/3} + d_p'^{2/3}\right)}\right)$	(25)

These modified models are plotted in Figure 3 using a constant drop size of $d_p = d_p' = 1.0$ mm and the numerical parameter values given in Table 3. Additionally, the critical approach velocity (CAV) model of Lehr and Mewes (2001) is illustrated in Figure 3 using a critical collision velocity of $v_{crit} = 45.8$ mm/s according to Equation (18).

As already discussed above, this representation shows clearly that (contrary to both the other models and the experimental data) the energy model predicts higher coalescence probability with higher velocity. The film drainage model of Coulaloglou and Tavlarides (1977) describes the experimental velocity dependency quite well, keeping in mind that Figure 3 only depicts the influence of collision velocity. The predicted decrease of coalescence efficiency by the CAV model is significantly smaller than observed in the experiments due to its hyperbolic formulation (Equation (18)). Additionally, the critical collision velocity is overestimated and should rather be $v_{crit} \leq 20$ mm/s. The models of Prince and Blanch (1990) and Henschke et al. (2002) show identical behaviour regarding the relative velocity: a coalescence probability of 100% is only reached at a relative velocity of zero. As coalescence of all colliding drops was observed at different velocities and parameter combinations, this prediction does not depict reality.

Overall, the relative velocity of the two drops during collision was approved to have a significant impact on the coalescence probability. A maximal collision velocity was found in this physical system above which no coalescence occurred. This first analysis of the dependency of coalescence efficiency models on relative velocity reveals that only the film drainage models describe the correct trend.

Drop diameter

The scattering of data points in Figure 3 for collision velocities $v_{coll} \leq v_{max}$ reveals that there are more influencing factors than the collision velocity. Thus, experimental data and coalescence efficiency models are analysed further with respect to the droplet diameters. In the systematic study of the drop size the target collision velocities were $v_{coll} = 25, 35$ and 45 mm/s. These low relative velocities could only be obtained with short droplet distances of around $h = 0.5, 1.0$ and 1.5 mm according to the solutions of Equation (20). At these short distances the drop detachment from the lower cannula induces fluctuations of the rise velocity and drop shape oscillations. Consequently, the collision velocities determined by image analysis varied significantly. In

order to visualize the results, the determined collision velocities were grouped in three intervals of 10 mm/s width: 20 mm/s $\leq v_{coll} \leq$ 30 mm/s, 30 mm/s $< v_{coll} \leq$ 40 mm/s and 40 mm/s $< v_{coll} \leq$ 50 mm/s.

In Figure 4 the analysed coalescence efficiency models versus the drop diameter are shown for a constant collision velocity $v_{coll} = 35$ mm/s assuming a collision of equally sized drops to achieve a two-dimensional representation. The used model parameters are identical to the ones used in Figure 3 (see Table 3). Additionally, experimental data from the corresponding velocity interval (30 mm/s $< v_{coll} \leq$ 40 mm/s) is shown in Figure 4: filled black dots represent experiments in which the colliding drop sizes were equal and grey circles indicate experiments with unequal drop sizes using the equivalent drop size d_{eq} according to Equation (9). It can be seen that the experimental coalescence probability increases with decreasing drop size especially for equally sized droplets but also if the equivalent drop diameter is calculated. The data point at $d_{eq} = 2.6$ mm resulting in a coalescence efficiency of $\lambda = 75$ % was regarded to be an outlier caused by the influence of drop oscillations (see discussion below and Figure 5b for details).

The model which depicts this behaviour correctly is the coalescence efficiency of Coulaloglou and Tavlarides (1977). All other models either show a contradictive trend (Henschke et al., 2002; Sovova, 1981) or estimate too high coalescence probabilities for the given drop diameters (Lehr and Mewes, 2001; Prince and Blanch, 1990). Also with variation of the numerical parameters the models of Prince and Blanch (1990) and Lehr and Mewes (2001) could not be fitted to the experimental data satisfactorily.

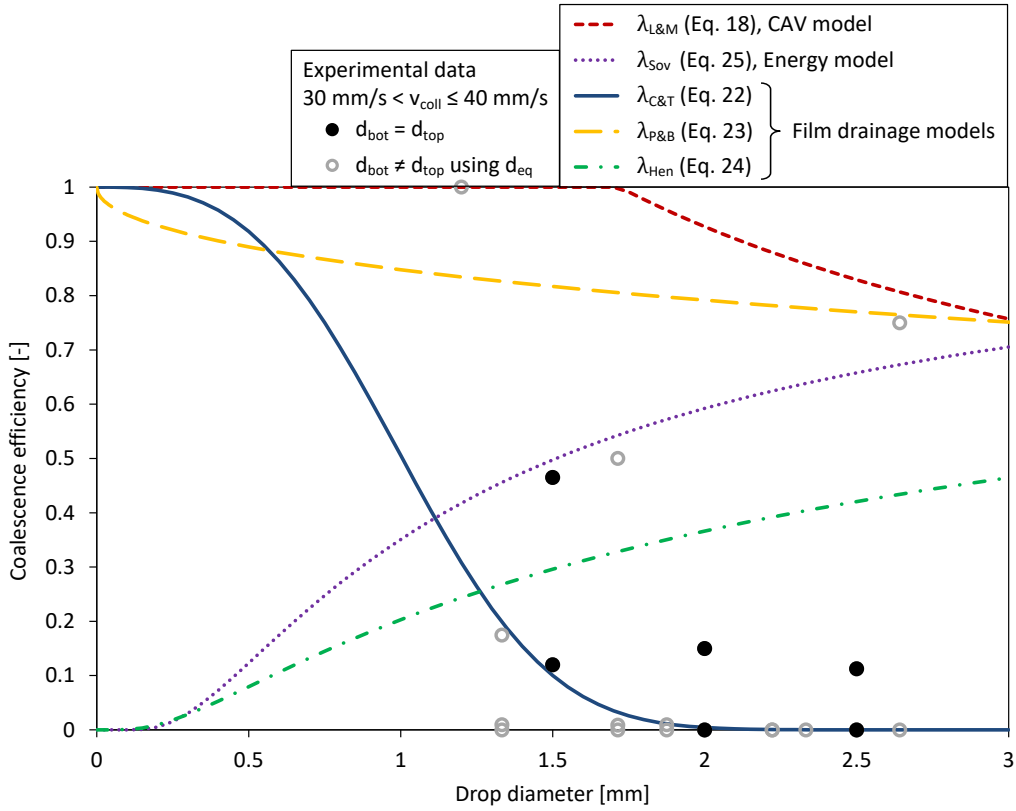

Figure 4: Coalescence probability vs. drop diameter for different coalescence efficiency models and experiments at collision velocities 30 mm/s $< v_{coll} \leq$ 40 mm/s.

The Coulaloglou and Tavlarides (1977) model could be fitted right between the black dots of the experimental data by using a parameter value $c_{2,c}$ with half of the value used here, but that would result in larger deviations in the three-dimensional plots shown below (Figure 5). Within the chosen intervals the coalescence probability is plotted versus the drop diameters d_{top} and d_{bot} in three-dimensional graphs in Figure 5. The experimental values are shown together with the film drainage model of Coulaloglou and Tavlarides (1977). The model parameter was adapted to $c_{2,c\ C\&T} = 2 \cdot 10^{12}\ \mathrm{m}^{-2}$ using these most detailed representations and the interval's mean velocity ($v_{coll} = 25, 35, 45$ mm/s), respectively. It can be seen that at the lowest velocities (20 mm/s $\leq v_{coll} \leq$ 30 mm/s, Figure 5a) the coalescence probability scatters significantly and the experimental values are higher than the prediction by the model especially for rising droplets of $d_{bot} = 2.5$ mm. As already discussed above, the low velocities required very small rise heights of the droplets (0.5 mm and below) which made the measurements challenging and susceptible to fluctuation of cannula detachment. Particularly, big drops ($d_{bot} = 2.5$ mm) showed distinct oscillations during the short rising path which have a significant influence on the coalescence probability (see discussion below). From the plotted Coulaloglou and Tavlarides (1977) model the characteristic dependency on drop sizes can be seen. The model predicts highest coalescence efficiency for a collision of two small equally sized droplets and lowest probability for a collision of two equally sized big drops. The collision of unequally sized drops results in higher coalescence probability if the difference between the drop sizes is bigger. This trend can also be noticed in the experiments with 30 mm/s $< v_{coll} \leq$ 40 mm/s (Figure 5b). If one neglects single outliers mostly caused by oscillating drops, the model fits the experimental data sufficiently. The same can be stated for the higher velocities (40 mm/s $< v_{coll} \leq$ 50 mm/s, Figure 5c).

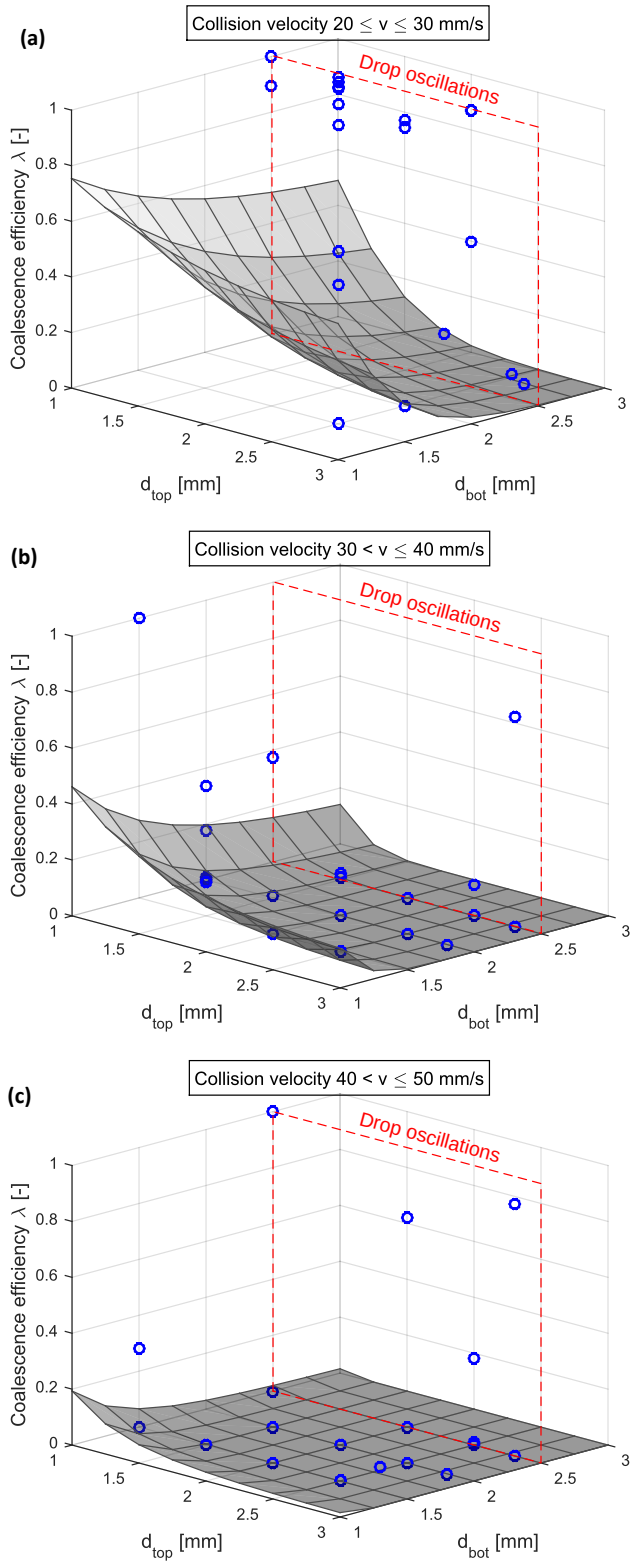

Figure 5: Three-dimensional visualisation of the dependency of coalescence probability on the drop sizes (d_{top}, d_{bot}) in experiments and applying the Coulaloglou and Tavlarides (1977) model with $c_{2,c\ C\&T} = 2 \cdot 10^{12}$ m^{-2}. To account for different collision velocities, the data is shown in three velocity intervals of 10 mm/s width.

The drop diameter is probably the most important influencing factor within the population balance equation because it is the only parameter which changes during an integral PBE over time in a given physical system. Using mean energy dissipation rates results in mean (and constant) relative velocities within the models. The drop size distribution changes over time by the drop breakage and coalescence rates which only change due to varying drop sizes. Therefore, it is remarkable that the influence of the drop diameter is depicted inconsistently and even contradictorily in the modelling approaches. This fact was also discussed by Kopriwa et al. (2012) and Kamp et al. (2016b) considering also additional coalescence models. The only model describing the correct tendencies of experimental data so far is the film drainage model of Coulaloglou and Tavlarides (1977).

A different frequently discussed parameter is the surface mobility. Due to the varying implementation of this boundary condition in film drainage models it results in significantly different models with altering dependencies on the influencing factors. The experimental data presented in this study was obtained with fully mobile interfaces (see section 3.1). In the opinion of the authors, the surface mobility indisputably has a significant impact on coalescence but should not vary the model dependency on important influencing factors like the drop size substantially. Apart from the discussed discrepancies in the coalescence efficiency models it should be noted that with all models somewhat meaningful simulation results might be obtained within the range of process conditions at which parameter estimation was performed. However, a sound extrapolation beyond this restricted range of process conditions is not possible. An important reason is that drop breakage and coalescence in general occur simultaneously and, thus, model deficiencies in PBE can deplete each other. Moreover, each submodel has (at least) one numerical fitting parameter which allows the adaption to desired experimental data. This shows the importance of the present validation method in this work. Coalescence efficiency submodels could be evaluated independently for the first time considering the impact of individual influencing parameters. Moreover, it was possible to determine the numerical parameter $c_{2,c}$ of the Coulaloglou and Tavlarides (1977) model based on independent single drop experiments.

Drop oscillations

Due to the detachment from the cannula the rising droplet shows significant shape oscillations for the first millimetres as already discussed in section 3.1. During detachment the drop is deformed and the interface tears off the cannula's rim. The interfacial tension drives the drop back to spherical shape which causes the mentioned oscillations. This effect cannot be avoided in the experimental set-up but once effective detachment parameters (flushed water volume and pump speed) are found, the drop deformations during detachment are reproducible for a series of sequences. However, repetition runs on a different day might require slightly different detachment parameters and the drop oscillations vary accordingly.

As already mentioned above, rising drops of sizes $d_p > 2.0\ mm$ showed significant oscillations after cannula detachment which resulted in the deviations in Figure 5. In Figure 6 the mean rise velocities of four sequences with identical drop sizes ($d_{top} = 1.5\ mm$, $d_{bot} = 2.5\ mm$) over small rise heights ($h < 0.6$ mm) are shown. Drop collisions occurred at heights where the graphs end. The four sequences differ slightly concerning detachment parameters and drop collision height which results in a collision velocity equal for two sequences respectively but differs in the oscillatory behaviour of the drops at collision. The standard deviations of the averaged sequences are relatively small and only shown for one graph exemplarily. The oscillation of the droplets can be

identified from the amplitudes of the mean rise velocity: on the one hand the drag coefficient changes by drop deformation and the actual three-dimensional deformations change the centroid of the two-dimensional image, on the other hand the image analysis seems to detect a slightly shifted drop centre due to different illumination and, thus, detection of the drop borders. Local minimal values in the mean rise velocity over height approximately correspond to a horizontal elongation and maximal values to a vertical elongation of the drop. The maximal and minimal diameters of the deformed drop reached approximately 2.5 ± 0.1 mm which corresponds to variations of $\pm 4\%$ of the drop diameter. Still, these fluctuations are significant as the drop rise heights are small ($h < 0.6$ mm).

The corresponding coalescence probabilities of the two sequences with equal collision velocities differ significantly. At a collision velocity of $v_{coll} \approx 24\ mm/s$ the coalescence probability results in $\lambda = 97.3\%$ and 36.3%. The higher collision velocity of $v_{coll} \approx 28\ mm/s$ yields coalescence probabilities of $\lambda = 95.3\%$ and 24.3%. It can be stated that the oscillation of the drops differ for the four experiments shown in Figure 6. However, the exact oscillatory state of the droplets during collision cannot be identified from the fluctuations of the mean rise velocity.

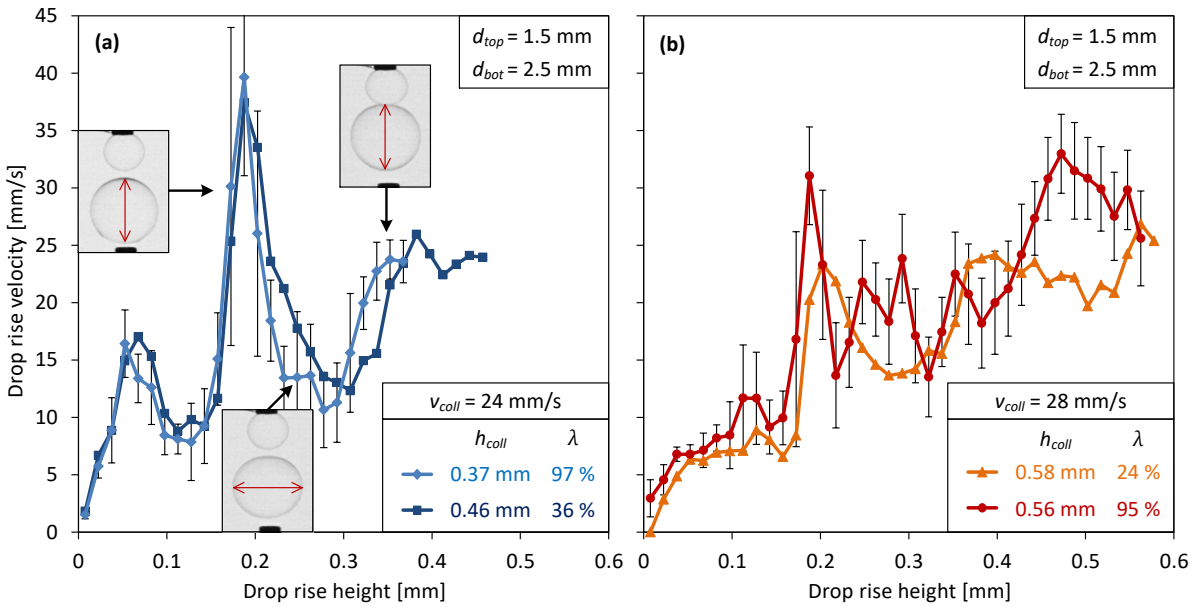

Figure 6: Evaluation of the impact of drop oscillation on coalescence probability by comparing trajectories of different experiments with equal collision velocities: (a) $v_{coll} = 24$ mm/s and (b) $v_{coll} = 28$ mm/s.

Scheele and Leng (1971) found that the oscillatory state of drops during collision had a significant impact on the coalescence probability in their experiments. The authors investigated anisole drops in water which collided horizontally in their test cell. Limited by the use of analogue high speed camera recordings only 23 high speed sequences could be recorded and analysed. The authors identified the maximal amplitude of the oscillation being 20% of the drops' diameter. Scheele and Leng (1971) found coalescence if the oscillatory state was changing from maximal horizontal elongation and transition to vertical elongation. In contrast, repulsion was reported if the drops collided at an oscillatory state around the maximal vertical elongation and transition to horizontal elongation. In the present analysis the amplitude of the oscillation was significantly smaller and a clear trend could not be found due to the limited analysis of mean values. Every single droplet shows slightly different oscillation behaviour due to small fluctua-

tions in the detachment from the cannula and other experimental conditions. To be able to develop conclusive statements of the oscillatory state influencing the coalescence probability it would be necessary to correlate the oscillation of every single collision with the coalescence or repulsion events. Unfortunately, the developed image analysis is not able to provide this information yet but will be done in future analysis.
In general, it can be confirmed already from these investigations based on mean values that the oscillatory state of the colliding drops has a significant influence on the coalescence probability. In technical applications with turbulent flow patterns these fluctuations are random and probably of no special interest in PBE simulations because the effect can be described by the statistical approaches of coalescence models. But for single drop investigations care has to be taken that the impact of drop oscillations does not superimpose other influencing factors.

3.3. Transfer to droplet swarms

The findings from the single drop investigations were used to simulate experiments in a lab scale stirred tank DN 150 (see section 2.1 for details) with the same physical system toluene/water at a disperse phase fraction of $\varphi = 10\%$. In these experiments the drops are about one order of magnitude smaller (200 – 600 µm) and the absolute flow velocities within the stirred tank are in the order of $v_{flow} \approx 1$ m/s (Maaß et al., 2009). But for coalescence the relative velocity of droplets flowing within the continuous flow is important and can be estimated by Equation (8). For the investigated stirred tank the relative velocities between the droplets result in $v_{rel} \approx 50 - 100$ mm/s using the mean energy dissipation rates within the whole vessel induced by the impeller (values see section 2.1). Hence, the relative velocities studied in the single drop investigations (section 3.2) were in the same relevant range. Drop shape oscillations of smaller drops are dampened by higher capillary forces due to higher relative surface, but turbulent fluctuations in the stirred tank induce pressure fluctuations on the drop surface which also deform the drops. Obviously, the local energy dissipation rate within the stirred tank differs significantly from this mean value (Maaß et al., 2009; Stoots and Calabrese, 1995) and, thus, relative velocities between the drops as well as breakage and coalescence rates vary depending on the position in the vessel (Park and Blair, 1975). Stoots and Calabrese (1995) found that the energy dissipation rates near the impeller tips can exceed 3 – 10 folds the mean energy dissipation rate within a stirred tank. Wu and Patterson (1989) estimated maximum energy dissipation rates in the trailing vortices being about 15 times higher than the mean energy dissipation rate. With CFD simulations Maaß et al. (2009) obtained a ratio of maximum and mean energy dissipation rate $\epsilon_{max}/\epsilon_{mean} = 25$. Park and Blair (1975) measured the drop size distribution at four positions in a stirred tank using the system MIBK/water. They found a change of drop size distribution from smaller drops near impeller to bigger drops in the circulation region. However, the observed difference in drop size was only around 16% between the regions. An explanation is that the zones of high energy dissipation rates are very small compared to the whole tank volume and high volume flow rates are passing these zones near the impeller. Additionally, in fully turbulent flow regime the whole tank is mixed intensively. Therefore, the deviations in drop size distribution are balanced fast within the stirred tank. Accordingly, Ritter and Kraume (2000) did not find significant dissimilarities between drop size distributions measured at different positions in a stirred tank using the system toluene/water. As a result, reasonable results can already be obtained using mean values in an integral simulation (Maaß et al., 2010). To keep the complexity and influence of other factors as small as possible, in this study an integral single

zone PBE simulation of the whole batch reactor with mean energy dissipation rate was performed.
The temperature difference of 5°C between single drop experiments and stirred vessel measurements does not influence the coalescence behaviour. The temperature influence was investigated (data not shown) but no significant differences could be found in coalescence probability of single drops even for higher temperature differences.

From single drop experiments the film drainage model of Coulaloglou and Tavlarides (1977) was identified to describe the coalescence probability satisfactorily for the investigated parameters in contrast to the other evaluated modelling approaches. In a first approach the breakage rate and the collision frequency were also modelled by the submodels proposed by Coulaloglou and Tavlarides (1977). Numerical parameters are needed to apply the population balance equation to a specific system. In literature a broad variety of parameter sets can be found (Maaß, 2011; Ribeiro et al., 2011) because interdependencies between the numerical parameters exist (Ribeiro et al., 2011). For that reason, different parameter combinations can lead to the same ratio between drop breakage and coalescence rate which results in identical simulations (at least in steady state). Ribeiro et al. (2011) discussed the proportional dependency between the pre-exponential parameters c_{1b} and c_{1c} for steady state simulations in detail. As drop breakage is not in the focus of this work but inevitable to simulate a stirred vessel, appropriate parameters (c_{1b}, c_{2b}) from the literature were used and compared (see Table 4): the original parameters of Coulaloglou and Tavlarides (1977), c_{1b} and c_{2b} from an earlier publication (Kamp and Kraume, 2015) and breakage parameters estimated from single drop experiments by Maaß and Kraume (2012). The numerical parameter of the coalescence probability model of Coulaloglou and Tavlarides (1977) was set to $c_{2c} = 2 \cdot 10^{12}\ \mathrm{m}^{-2}$ according to the single drop experiments discussed in section 3.2. Due to the fixed determination of c_{2c} the parameter c_{1c} must be adapted in order to avoid a shift between the breakage and coalescence rate. Therefore, primarily the numerical parameter c_{1c} was fitted to experiments in the stirred vessel at a stirrer frequency of $n = 550\ \mathrm{min}^{-1}$. The resulting parameters sets are shown in Table 4.

The experimentally determined Sauter mean diameters d_{32} within the stirred vessel for different stirrer frequencies ($n = 400, 550, 700\ \mathrm{min}^{-1}$) are shown in Figure 7 together with the performed simulations. It can be seen that the steady state (constant drop size distribution and, therefore, constant Sauter mean diameter) is reached within the first seconds of the experiments. The experimental procedure did not allow drop size distribution measurements before the first data points because the triggering and image acquisition with the endoscope probe took at least 30 seconds. The logarithmic scale was chosen to depict the different transient behaviour of the simulations in the first seconds after start of the impeller. The simulations using the adapted parameters from Coulaloglou and Tavlarides (1977) (parameter set (b)) and Kamp and Kraume (2015) (parameter set (d)) could be fitted well to the data with a stirrer frequency $n = 550\ \mathrm{min}^{-1}$. But significant deviations between the experimental data and simulations with different stirrer frequencies can be observed. The difference between simulation and experiment data at $n = 700\ \mathrm{min}^{-1}$ is around $-20\ \mu m$ from the mean value which almost lies within the experimental uncertainty (cf. variations of steady state d_{32}). The Sauter mean diameter at $n = 400\ \mathrm{min}^{-1}$ is overestimated by about 70 µm ($\approx 15\%$). The overall root-mean-square deviations for both parameter sets are about $RSMD = 50$ µm (see Table 6). The deviations with variation of the energy dissipation rate (here induced by the stirrer frequency) was also reported in earlier investigations (Kamp and Kraume, 2015; Maaß et al., 2010). It is remarkable that the two

simulations using the adapted parameter sets of Coulaloglou and Tavlarides (1977) and Kamp and Kraume (2015) result in nearly identical steady states of d_{32} although the parameters c_{1b} and c_{1c} vary by several orders of magnitude. But the ratio between the parameters c_{1b}/c_{1c} and the value of c_{2b} do not vary considerably which confirms the findings of Ribeiro et al. (2011). The absolute values of c_{1b} and c_{1c} influence the transient behaviour significantly. The by two orders of magnitude higher breakage and coalescence rate of the adapted Coulaloglou and Tavlarides (1977) parameters show a proportionally faster decrease of d_{32} over time. This also shows that the transient behaviour of a simulation can be adapted easily using this dependency. This applies in the same manner to the breakage rate as well as to the coalescence rate of PBE simulations. In Figure 8 breakage and coalescence rate of the Coulaloglou and Tavlarides (1977) model are shown using the parameter set (b). The coalescence rate is plotted for collisions of equally sized drops in order to allow a two-dimensional representation (cf. Figure 5). Variations of the pre-exponential parameters c_{1b} and c_{1c} change the values of the breakage and coalescence rate proportionally (vertically in Figure 8). A shift of the graphs to smaller or bigger drop sizes (horizontally in Figure 8) can be achieved by altering the exponential parameters c_{2b} and c_{2c} which does not vary the maximum values of the rates. From the representation in Figure 8 already a rough estimation of the resulting drop sizes can be given: in steady state the breakage and coalescence rate have to result in non-zero values at these drop sizes. Smaller drop sizes would only coalesce and bigger drop sizes would only break. In Figure 8 breakage and coalescence rate both result in significant values for drop sizes between 200 µm and 800 µm varying with the impeller speed. It becomes apparent that the values of coalescence and breakage rate differ by ten orders of magnitude. This has to be explained by the definition of the PBE (Equation (5)): in breakage events only one mother drop is involved which is represented by the number density function $f(d_p, t)$ in Equation (5) whereas in case of coalescence always two mother drops interact and, thus, the number density function $f(d_p, t)$ appears two times in the coalescence source terms in Equation (5). Considering that there are several billions (10^9) of drops per cubic meter present in the simulations, the resulting death and birth terms of coalescence and breakage are in the same order of magnitude.

The simulations using the breakage parameters from single drop experiments of Maaß and Kraume (2012) (parameter set (f)) do not describe the experimental data due to the low breakage rate and, thus, too slow transient behaviour ($RSMD = 158$ µm). The experimental steady state values were not reached in these simulations before a simulation time of about 14 hours. The slow transient behaviour is caused by a too small breakage rate which is the determining part during the decrease of drop sizes. Maaß and Kraume (2012) only investigated the drop breakage and, thus, did not determine coalescence parameters. It has to be mentioned that the sole breakage rate model of Coulaloglou and Tavlarides (1977) was not focus of their work and no parameter set was found to fit the single drop experiments in a satisfying manner. Thus, it is not surprising that these simulations did not provide accurate results. By increasing the breakage and coalescence rate proportionally it was possible to find parameter values of c_{1b} and c_{1c} (parameter set (g)) with which the steady state d_{32} is reached after one minute. The description of the experimental data is comparable to the simulations discussed above (parameter sets (b) and (d)) with a mean deviation of $RSMD = 59$ µm.
Maaß and Kraume (2012) achieved better breakage parameter fits by combining their developed breakage time with other breakage probability models (Alopaeus et al., 2002; Chen et al., 1998).

In Table 4 additional parameter sets from different authors are given for comparison to the parameter sets obtained in this study. Most authors in Table 4 investigated the drop size distribution in stirred vessels using various physical systems. Two authors studied different set-ups: Azizi and Taweel (2011) applied static mixers to create the liquid/liquid dispersion, and Jildeh et al. (2014) determined parameters for Kühni extraction columns with several oil/water systems (using a different breakage model). The parameters from literature fit quite well to the parameter sets obtained in this study. Especially the coalescence efficiency parameter $c_{2,c} = 2 \cdot 10^{12}$ determined by single drop experiments in section 3.2 fits in the range of parameter values available in literature.

The apparent deviations of the simulations concerning the impeller frequency are mainly caused by the breakage kernel of the Coulaloglou and Tavlarides (1977) model. The authors tested several different coalescence submodels (data not shown) and were not able to reduce the dependency on the energy input. Therefore, the breakage submodel of Chen et al. (1998) was implemented which performed better in the single drop breakage experiments of Maaß and Kraume (2012). As can be seen in Figure 8 the breakage rate of Chen et al. (1998) shows a less pronounced dependency on the energy dissipation rate (or stirrer frequency) than the breakage rate of Coulaloglou and Tavlarides (1977). The numerical parameter c_{1c} as well as the additional breakage parameter c_{3b} were fitted to the experiments with stirrer frequency $n = 550$ min^{-1}. Additionally, the pre-exponential parameters c_{1b} and c_{1c} had to be increased by two orders of magnitude (parameter set (p)) to depict the fast transient behaviour of the experiments (see Table 5 and Figure 7). The lower impact of energy dissipation rate on the breakage rate of Chen et al. (1998) decreases the variation of steady state Sauter mean diameters d_{32} with stirrer frequency. Therefore, the simulations predict all experiments within the experimental deviations and result in a mean deviation of $RSMD = 15$ µm.

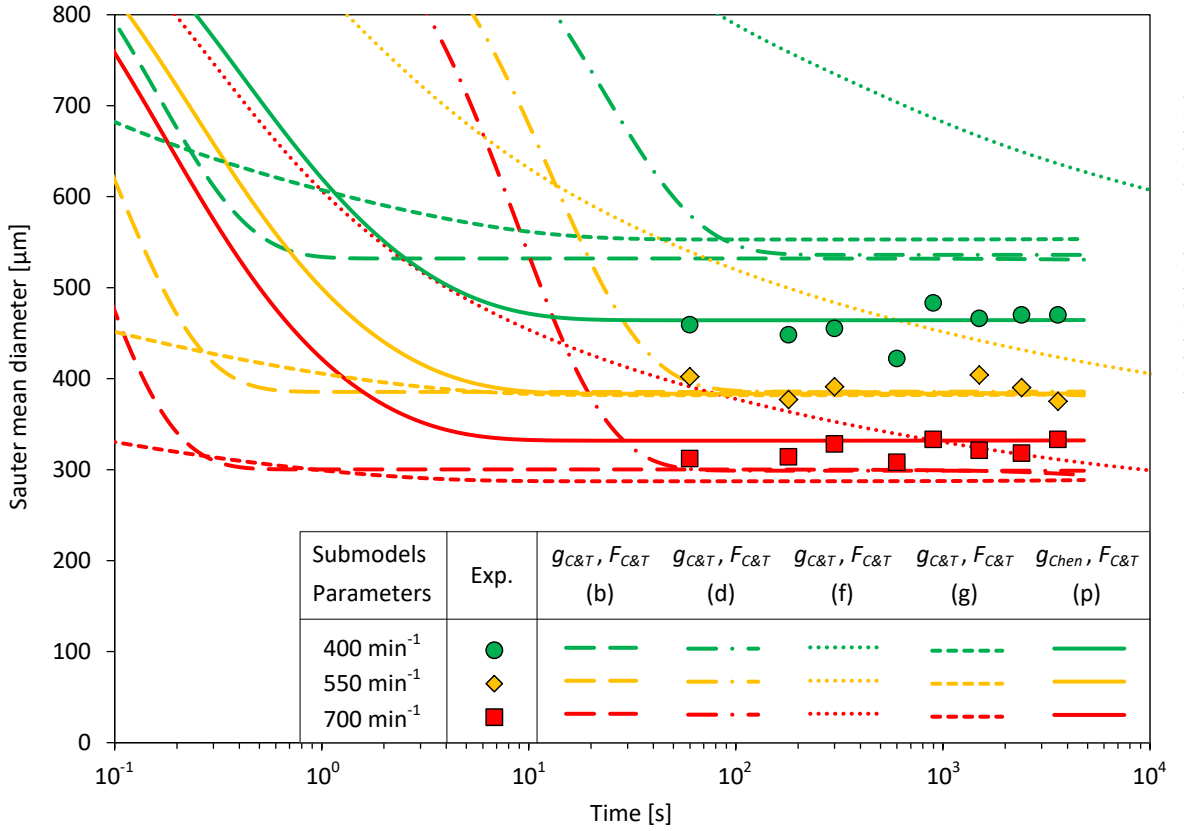

Figure 7: Experimental data and simulations of Sauter mean diameter d_{32} in a stirred tank (DN150, Rushton turbine, toluene/water) versus time for different stirrer frequencies. Different submodels were used: breakage rate of Coulaloglou and Tavlarides (1977) $g_{C\&T}$ (Equation (10)); breakage rate of Chen et al. (1998) g_{Chen} (Equation (11)); coalescence rate of Coulaloglou and Tavlarides (1977) $F_{C\&T} = \xi_{C\&T} \cdot \lambda_{C\&T}$ (Equations (13) and (14)) with different parameters sets (see Table 4 and Table 5).

Table 4: Numerical parameters for complete Coulaloglou and Tavlarides (1977) model from different authors and the adapted coalescence parameters in this study. For comparison additional parameter sets from different authors are given.

Numerical parameters	***set***	$c_{1,b}$	$c_{2,b}$	$c_{1,c}$	$c_{2,c}$ $[m^{-2}]$
Coulaloglou & Tavlarides (1977)					
original parameters	(a)	$5.3975 \cdot 10^{-1}$	$4.3936 \cdot 10^{-2}$	$3.7783 \cdot 10^{-6}$	$4.4963 \cdot 10^{13}$
adapted parameters	(b)	$5.3975 \cdot 10^{-1}$	$4.3936 \cdot 10^{-2}$	$1.2980 \cdot 10^{-1}$	$2.0 \cdot 10^{12}$
Kamp & Kraume (2015)					
original parameters	(c)	$4.8701 \cdot 10^{-3}$	$5.5199 \cdot 10^{-2}$	$1.1878 \cdot 10^{-1}$	$3.8591 \cdot 10^{13}$
adapted parameters	(d)	$4.8701 \cdot 10^{-3}$	$5.5199 \cdot 10^{-2}$	$7.3789 \cdot 10^{-4}$	$2.0 \cdot 10^{12}$
Maaß & Kraume (2012)					
original parameters	(e)	$9.1 \cdot 10^{-1}$	$3.9 \cdot 10^{-1}$	-	-
adapted parameters	(f)	$9.1 \cdot 10^{-1}$	$3.9 \cdot 10^{-1}$	$2.0309 \cdot 10^{-7}$	$2.0 \cdot 10^{12}$
adapted parameters	(g)	$9.1 \cdot 10^{3}$	$3.9 \cdot 10^{-1}$	$2.0309 \cdot 10^{-3}$	$2.0 \cdot 10^{12}$
Hsia and Tavlarides (1980)	(h)	$4.87 \cdot 10^{-3}$	$5.52 \cdot 10^{-2}$	$2.17 \cdot 10^{-4}$	$2.28 \cdot 10^{13}$
Bapat and Tavlarides (1985)	(i)	$4.81 \cdot 10^{-3}$	$8.00 \cdot 10^{-2}$	$1.90 \cdot 10^{-3}$	$2.00 \cdot 10^{12}$
Gäbler et al. (2006)	(j)	$6.14 \cdot 10^{-4}$	$5.70 \cdot 10^{-2}$	$1.50 \cdot 10^{-4}$	$2.56 \cdot 10^{12}$
Azizi and Taweel (2011)	(k)	$8.60 \cdot 10^{-1}$	4.10	$4.00 \cdot 10^{-2}$	$1.00 \cdot 10^{10}$
Ribeiro et al. (2011)	(l)	$4.664 \cdot 10^{-3}$	$3.175 \cdot 10^{-2}$	$1.00 \cdot 10^{-3}$	$5.446 \cdot 10^{6}$
Maaß (2011)	(m)	$2.30 \cdot 10^{-3}$	$3.08 \cdot 10^{-2}$	$5.70 \cdot 10^{-4}$	$7.11 \cdot 10^{12}$
Jildeh et al. (2014)	(n)	-	-	$5.50 \cdot 10^{-2}$	$1.33 \cdot 10^{11}$

Table 5: Numerical parameters for breakage model of Chen et al. (1998) combined with Coulaloglou and Tavlarides (1977) coalescence rate model.

Numerical parameters	***set***	$c_{1,b}$	$c_{2,b}$	$c_{3,b}$	$c_{1,c}$	$c_{2,c}$ $[m^{-2}]$
Chen et al. (1998)						
original parameters	(o)	$6.040 \cdot 10^{-1}$	$1.136 \cdot 10^{-3}$	$7.849 \cdot 10^{-3}$	-	-
adapted parameters	(p)	$6.040 \cdot 10^{1}$	$1.136 \cdot 10^{-3}$	$1.789 \cdot 10^{2}$	$3.189 \cdot 10^{-3}$	$2.0 \cdot 10^{12}$

Table 6: Root-mean-square deviations of Sauter mean diameter $RSMD(d_{32})$ between experiments and simulations using different numerical parameter sets (see Table 4 and Table 5) and breakage submodels (Coulaloglou and Tavlarides (1977) and Chen et al. (1998)).

$F(d_p, d_p')$	$g(d_p)$	***parameter set***	***n = 400 min^{-1}***	***n = 550 min^{-1}***	***n = 700 min^{-1}***	***total***
C&T	C&T	(b)	74.7 µm	12.0 µm	24.1 µm	45.8 µm
C&T	C&T	(d)	85.5 µm	10.0 µm	23.7 µm	51.5 µm
C&T	C&T	(f)	256.4 µm	89.5 µm	36.8 µm	158.2 µm
C&T	C&T	(g)	95.5 µm	13.6 µm	34.5 µm	59.1 µm
C&T	Chen	(p)	17.9 µm	12.8 µm	14.2 µm	15.1 µm

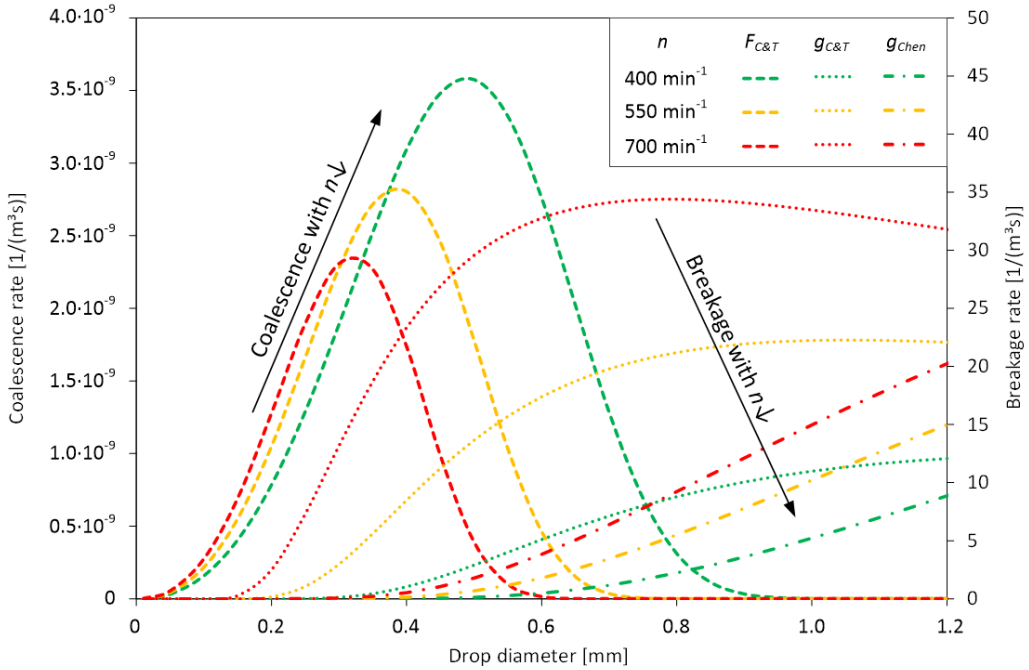

Figure 8: Breakage and coalescence rates at varying stirrer frequencies using the models of Coulaloglou and Tavlarides (1977) and Chen et al. (1998) with the parameter sets (b) and (p) given in Table 4 and Table 5. (Corrected erratum: increasing / decreasing stirrer frequency: n↓ / n↑)

Overall, the experimental data could be simulated adequately using the coalescence efficiency parameter $c_{2,c}$ from the single drop experiments which is quite intriguing keeping in mind that these single drop experiments were a simplification of the complex interactions within turbulent droplet swarms. Moreover, the investigated single drops were about one order of magnitude larger than the measured drop sizes in the stirred vessel. This shows that the systematic investigation of single drop coalescence provided the successful determination of the coalescence parameter $c_{2,c}$ independently from the drop breakage for the first time. Before, the numeric parameters were fitted together to drop size distributions of systems in which drop breakage and coalescence occurred simultaneously. Due to interdependencies between these parameters no distinct and independent parameter could be determined in the past. Additionally, only small amounts of the investigated process liquids are necessary for single drop experiments in contrast to lab or pilot plant scale experiments with dynamic drop swarms.

4. Summary and outlook

Investigations using PBE consist of various submodels with numerical parameters which are not determined a priori. An independent evaluation of submodels (especially for coalescence) was not possible up to now. Commonly, the parameters are fitted to (transient) drop size distributions of dynamic multiphase systems in which breakage and coalescence occur simultaneously. Additionally, the numerical parameters show interdependencies and parameter sets can be found in literature with divergent values in several orders of magnitude. Due to the lack of well proved PBE models it might occur that inconsistencies in submodels compensate each other which leads to proper results for the fitted case but does not allow any extrapolation. Thus, fitted

simulations to experimental data do not provide a reliable framework for extrapolation and scale-up without sound validation.

This work provides experimental single drop data as a basis for model validation regarding different important influencing factors on coalescence individually: relative collision velocity (or energy dissipation rate) and drop diameter. Additionally, the impact of drop oscillations on coalescence probability is discussed. Based on the single drop data, five different coalescence efficiency models were evaluated and discussed. The film drainage model of Coulaloglou and Tavlarides (1977) describes all investigated influencing factors in the correct manner. Independent from drop breakage the numerical parameter of coalescence efficiency $c_{2,c}$ could be fitted to single drop data for the first time.

With the obtained parameter $c_{2,c}$ it was possible to successfully simulate a stirred vessel using the PBE framework. The apparent interdependencies between numerical parameters are shown and discussed. Additionally, results from earlier single drop breakage investigations were considered which increased the accuracy of the simulation results. In conclusion, a successful scale-up from single drop experiments to the description of turbulent droplet swarms in a stirred vessel was performed. The presented results show that a sound scale-up is possible using population balance equation simulations even without maintaining geometric similarity.

In ongoing studies, the presented systematic coalescence probability investigations can be used to evaluate other modelling approaches and develop new ones. Additionally, further influencing factors (e.g., phase properties, species and concentration of surfactants and ions) can be investigated systematically using the presented methods. Based on sound experimental data, reliable coalescence models can be developed which might describe the important influencing factors properly and allow a robust extrapolation and equipment design in industrial scale.

Acknowledgements

The authors kindly thank the student workers Alexander Malik and Stefanie Brekow who contributed substantially to the experimental data shown in this work as well as Dorothea Löffler and Gregor Kendzierski who developed the image analysis methods used in this work. Additionally, the authors kindly thank Stephanie Nachtigall and Franziska Michalski for providing the experimental data of the stirred tank measurements. Financial support provided by the German Research Foundation (DFG) within the project KR 1639/19-2 is gratefully acknowledged.

Nomenclature

Latin letters

$A_{1,2,3}$	Hamaker constant	[N m]
$c_{1,b}$	numerical parameter in PBE: breakage rate	[-]
$c_{2,b}$	numerical parameter in PBE: breakage rate	[-]
$c_{1,c}$	numerical parameter in PBE: collision frequency	[-]
$c_{2,c}$	numerical parameter in PBE: coalescence efficiency	various
c_β	standard deviation tolerance	[-]
C_D	drag coefficient	[-]
d_{32}	Sauter mean diameter	[m]
d_{bot}	bottom droplet diameter	[m]
d_{eq}	equivalent droplet diameter	[m]
d_i	impeller diameter	[m]
d_μ	mean diameter of Gaussian drop size distribution	[m]
d_σ	standard deviation of Gaussian drop size distribution	[m]
d_p, d_p', d_p''	particle / droplet diameter, differentiation between several drops by apostrophe(s): ′	[m]
$d_{p,max}$	maximal particle / droplet diameter	[m]
d_{top}	top droplet diameter	[m]
D_t	tank diameter	[m]
f	number density function	[m^{-3}]
F	coalescence rate	[m^3/s]
g	breakage rate	[s^{-1}]
g	gravitational acceleration	[m/s^2]
h	drop rise height	[m]
h_{coll}	drop rise height at collision	[m]
h_i	height of impeller installation (from bottom)	[m]
H_t	tank height	[m]
m	number of values	[-]
M	mass	[kg]
n	stirrer frequency	[min^{-1}]
n_d	number of daughter drops after breakage event: 2	[-]
Ne	Power / Newton number	[-]
P	power input	[W]
Re	Reynolds number	[-]
$s_{collision}$	drop separation distance at collision	[m]
t	time	[s]
$t_{contact}$	contact time of two drops	[s]
v	velocity	[m/s]

v_{coll}	relative collision velocity between drops	[m/s]
v_{crit}	critical collision velocity	[m/s]
v_{flow}	absolute flow velocity	[m/s]
v_{max}	maximal collision velocity	[m/s]
v_p	particle / droplet rise velocity	[m/s]
v_{rel}	relative velocity between drops (at collision)	[m/s]
v_t	terminal rise velocity	[m/s]
V_p	particle / droplet volume	[m³]
V_μ	mean value of daughter drop volume distribution	[m³]
V_σ	standard deviation of daughter drop volume distribution	[m³]
V_t	tank volume	[m³]
X_i	experimental value	various
$\hat{X}_i$	simulation result	various

Greek letters

α	virtual mass acceleration factor	[-]
β	daughter drop size distribution	[-]
ϵ	energy dissipation rate	[m²/s³]
ϵ_{max}	maximum energy dissipation rate	[m²/s³]
ϵ_{mean}	mean energy dissipation rate	[m²/s³]
γ	interfacial tension	[N/m]
λ	coalescence efficiency / probability	[-]
μ_c	continuous phase dynamic viscosity	[Pa s]
μ_d	disperse phase dynamic viscosity	[Pa s]
μ_{disp}	dynamic viscosity of dispersion	[Pa s]
μ^*	dynamic viscosity ratio	[-]
φ	phase fraction	[-]
ϱ_c	continuous phase density	[kg/m³]
ϱ_d	disperse phase density	[kg/m³]
ϱ_{disp}	density of dispersion	[kg/m³]
ϑ	temperature	[°C]
ξ	collision frequency	[m³/s]

Abbreviations

C&T	Coulaloglou and Tavlarides (1977)
CAV	Critical approach velocity
CFD	Computer fluid dynamics
Chen	Chen et al. (1998)
Hen	Henschke et al. (2002)

L&M	Lehr & Mewes (2001)
MIBK	Methyl isobutyl ketone
P&B	Prince & Blanch (1990)
PBE	Population balance equation(s)
PTFE	Polytetrafluoroethylene
RMSD	Root-mean-square deviation
Sov	Sovova (1981)

References

Alopaeus, V., Koskinen, J., Keskinen, K.I., Majander, J., 2002. Simulation of the population balances for liquid-liquid systems in a nonideal stirred tank. Part 2 - parameter fitting and the use of the multiblock model for dense dispersions. Chem. Eng. Sci. 57, 1815–1825. doi:10.1016/S0009-2509(02)00067-2

Attarakih, M.M., Bart, H.-J., Faqir, N.M., 2004. Numerical solution of the spatially distributed population balance equation describing the hydrodynamics of interacting liquid-liquid dispersions. Chem. Eng. Sci. 59, 2567–2592. doi:10.1016/j.ces.2004.03.005

Azizi, F., Taweel, A.M. Al, 2011. Turbulently flowing liquid-liquid dispersions. Part I: Drop breakage and coalescence. Chem. Eng. J. 166, 715–725. doi:10.1016/j.cej.2010.11.050

Bapat, P.M., Tavlarides, L.L., 1985. Mass transfer in a liquid-liquid CFSTR. AIChE J. 31, 659–666. doi:10.1002/aic.690310416

Bart, H.-J., Garthe, D., Grömping, T., Pfennig, A., Schmidt, S., Stichlmair, J., 2006. Vom Einzeltropfen zur Extraktionskolonne. Chem. Ing. Tech. 78, 543–547. doi:10.1002/cite.200500146 (*in German*)

Brauer, H., Mewes, D., 1972. Strömungswiderstand sowie stationärer Stoff- und Wärmeübergang an Blasen und Tropfen. Chemie Ing. Techn. 44, 953–956. doi:10.1002/cite.330441513

Butt, H.-J., Graf, K., Kappl, M., 2003. Physics and Chemistry of Interfaces (Physics Textbook). Wiley-VCH, Weinheim. doi:10.1002/3527602313

Chen, Z., Prüss, J., Warnecke, H.-J., 1998. A population balance model for disperse systems: Drop size distribution in emulsion. Chem. Eng. Sci. 53, 1059–1066. doi:10.1016/s0009-2509(97)00328-x

Chesters, A.K., 1991. The modeling of coalescence processes in fluid-liquid dispersions: a review of current understanding. Trans. Inst. Chem. Eng. 69, 259–270. (*Journal also referred as: Chem. Eng. Res. Des.*)

Coulaloglou, C.A., Tavlarides, L.L., 1977. Description of interaction processes in agitated liquid-liquid dispersions. Chem. Eng. Sci. 32, 1289–1297. doi:10.1016/0009-2509(77)85023-9

Feng, Z.-G., Michaelides, E.E., 2001. Drag Coefficients of Viscous Spheres at Intermediate and High Reynolds Numbers. J. Fluids Eng. 123, 841–849. doi:10.1115/1.1412458

Frisch, U., 1995. Turbulence: The Legacy of A. N. Kolmogorov. Cambridge University Press, Cambridge.

Gäbler, A., Wegener, M., Paschedag, A.R., Kraume, M., 2006. The effect of pH on experimental and

simulation results of transient drop size distributions in stirred liquid-liquid dispersions. Chem. Eng. Sci. 61, 3018–3024. doi:10.1016/j.ces.2005.10.072

Ghotli, R.A., Raman, A.A.A., Ibrahim, S., Baroutian, S., 2013. Liquid-liquid Mixing In Stirred Vessels: A Review. Chem. Eng. Commun. 200, 595–627. doi:10.1080/00986445.2012.717313

Henschke, M., Schlieper, L.H., Pfennig, A., 2002. Determination of a coalescence parameter from batch-settling experiments. Chem. Eng. J. 85, 369–378. doi:10.1016/S1385-8947(01)00251-0

Hinze, J.O., 1955. Fundamentals of the hydrodynamic mechanism of splitting in dispersion processes. AIChE J. 1, 289–295. doi:10.1002/aic.690010303

Howarth, W.J., 1964. Coalescence of drops in a turbulent flow field. Chem. Eng. Sci. 19, 33–38. doi:10.1016/0009-2509(64)85003-x

Hsia, M.A., Tavlarides, L.L., 1980. A simulation model for homogeneous dispersions in stirred tanks. Chem. Eng. J. 20, 225–236. doi:10.1016/0300-9467(80)80007-4

Hulburt, H.M., Katz, S., 1964. Some problems in particle technology. Chem. Eng. Sci. 19, 555–574. doi:10.1016/0009-2509(64)85047-8

Jildeh, H.B., Attarakih, M., Mickler, M., Bart, H.-J., 2014. Parameter optimisation and validation for droplet population balances. Can. J. Chem. Eng. 92, 210–219. doi:10.1002/cjce.21892

Kamp, J., Hänsch, R., Kendzierski, G., Kraume, M., Hellwich, O., 2016a. Automated image analysis for trajectory determination of single drop collisions. Comput. Chem. Eng.

Kamp, J., Kraume, M., 2015. Coalescence efficiency model including electrostatic interactions in liquid/liquid dispersions. Chem. Eng. Sci. 126, 132–142. doi:10.1016/j.ces.2014.11.045

Kamp, J., Kraume, M., 2014. Influence of drop size and superimposed mass transfer on coalescence in liquid/liquid dispersions - Test cell design for single drop investigations. Chem. Eng. Res. Des. 92, 635–643. doi:10.1016/j.cherd.2013.12.023

Kamp, J., Villwock, J., Kraume, M., 2016b. Drop coalescence in technical liquid/liquid applications: a review on experimental techniques and modeling approaches. Rev. Chem. Eng. doi:10.1515/revce-2015-0071 (*in press*)

Kolmogorov, A.N., 1941. The Local Structure of Turbulence in Incompressible Viscous Fluid for Very Large Reynolds Numbers. Dokl. Akad. Nauk SSSR 30, 299. (*Reprint and translation: Proc. R. Soc. Lond. A (1991), 434(1890), pp. 9-13, http://www.jstor.org/stable/51980*)

Kopriwa, N., 2014. Quantitative Beschreibung von Koaleszenzvorgängen in Extraktionskolonnen. RWTH Aachen. (*in German*)

Kopriwa, N., Buchbender, F., Ayesteran, J., Kalem, M., Pfennig, A., 2012. A Critical Review of the Application of Drop-Population Balances for the Design of Solvent Extraction Columns: I. Concept of Solving Drop-Population Balances and Modelling Breakage and Coalescence. Solvent Extr. Ion Exch. 30, 683–723. doi:10.1080/07366299.2012.700598

Lasheras, J.C., Eastwood, C., Martinez-Bazan, C., Montanes, J.L., 2002. A review of statistical models for the break-up of an immiscible fluid immersed into a fully developed turbulent flow. Int. J. Multiph. Flow 28, 247–278. doi:10.1016/s0301-9322(01)00046-5

Lehr, F., Mewes, D., 2001. A transport equation for the interfacial area density applied to bubble

columns. Chem. Eng. Sci. 56, 1159–1166. doi:10.1016/S0009-2509(00)00335-3

Lehr, F., Millies, M., Mewes, D., 2002. Bubble-Size distributions and flow fields in bubble columns. AIChE J. 48, 2426–2443. doi:10.1002/aic.690481103

Liao, Y., Lucas, D., 2010. A literature review on mechanisms and models for the coalescence process of fluid particles. Chem. Eng. Sci. 65, 2851–2864. doi:10.1016/j.ces.2010.02.020

Liao, Y., Lucas, D., 2009. A literature review of theoretical models for drop and bubble breakup in turbulent dispersions. Chem. Eng. Sci. 64, 3389–3406. doi:10.1016/j.ces.2009.04.026

Maaß, S., 2011. Experimental analysis, modeling and simulation of drop breakage in agitated turbulent liquid/liquid-dispersions. Technische Universität Berlin, Chair of Chemical and Process Engineering.

Maaß, S., Kraume, M., 2012. Determination of breakage rates using single drop experiments. Chem. Eng. Sci. 70, 146–164. doi:10.1016/j.ces.2011.08.027

Maaß, S., Metz, F., Rehm, T., Kraume, M., 2010. Prediction of drop sizes for liquid-liquid systems in stirred slim reactors--Part I: Single stage impellers. Chem. Eng. J. 162, 792–801.

Maaß, S., Rehm, T., Kraume, M., 2011a. Prediction of drop sizes for liquid/liquid systems in stirred slim reactors - Part II: Multi stage impellers. Chem. Eng. J. 168, 827–838. doi:10.1016/j.cej.2011.01.084

Maaß, S., Wollny, S., Sperling, R., Kraume, M., 2009. Numerical and experimental analysis of particle strain and breakage in turbulent dispersions. Chem. Eng. Res. Des. 87, 565–572. doi:10.1016/j.cherd.2009.01.002

Maaß, S., Wollny, S., Voigt, A., Kraume, M., 2011b. Experimental comparison of measurement techniques for drop size distributions in liquid/liquid dispersions. Exp. Fluids 50, 259–269. doi:10.1007/s00348-010-0918-9

Misek, T., Berger, R., Schröter, J., 1985. Standard test systems for liquid extraction, 2nd Ed. ed, EFCE Publication Series. The Institution of Chemical Engineers, Rugby, UK, Rugby, UK.

Park, J.Y., Blair, L.M., 1975. Effect of coalescence on drop size distribution in an agitated liquid-liquid dispersion. Chem. Eng. Sci. 30, 1057–1064.

Prince, M.J., Blanch, H.W., 1990. Bubble coalescence and break-up in air-sparged bubble columns. AIChE J. 36, 1485–1499. doi:10.1002/aic.690361004

Princen, H.M., 1969. The equilibrium shape of interfaces, drops and bubbles. Rigid and deformable particles and interfaces, in: Matijevic, E. (Ed.), Surface and Colloid Science. Wiley-Interscience, New York, pp. 1–84.

Ramkrishna, D., 2000. Population Balances: Theory and Applications to Particulate Systems in Engineering. Academic Press, San Diego.

Randolph, A.D., Larson, M.A., 1962. Transient and steady state size distributions in continuous mixed suspension crystallizers. AIChE J. 8, 639–645. doi:10.1002/aic.690080515

Ribeiro, M.M., Regueiras, P.F., GuimaraÌfes, M.M.L., Madureira, C.M.N., Cruz_Pinto, J.J.C., 2011. Optimization of Breakage and Coalescence Model Parameters in a Steady-State Batch Agitated Dispersion. Ind. Eng. Chem. Res. 50, 2182–2191. doi:10.1021/ie100368t

Ritter, J., Kraume, M., 2000. On-line Measurement Technique for Drop Size Distributions in Liquid/Liquid Systems at High Dispersed Phase Fractions. Chem. Eng. Technol. 23, 579–

581. doi:10.1002/1521-4125(200007)23:7<579::AID-CEAT579>3.0.CO;2-Y

Scheele, G.F., Leng, D.E., 1971. An experimental study of factors which promote coalescence of two colliding drops suspended in water - I. Chem. Eng. Sci. 26, 1867–1879. doi:10.1016/0009-2509(71)86030-X

Simon, M., 2004. Koaleszenz von Tropfen und Tropfenschwärmen. Technische Universität Kaiserslautern, Chair of Separation Science and Technology. (*in German*)

Solsvik, J., Jakobsen, H.A., 2016. A review of the statistical turbulence theory required extending the population balance closure models to the entire spectrum of turbulence. AIChE J. 62, 1795–1820. doi:10.1002/aic.15128

Solsvik, J., Tangen, S., Jakobsen, H.A., 2013. On the constitutive equations for fluid particle breakage. Rev. Chem. Eng. 29. doi:10.1515/revce-2013-0009

Sovova, H., 1981. Breakage and coalescence of drops in a batch stirred vessel - II comparison of model and experiments. Chem. Eng. Sci. 36, 1567–1573. doi:10.1016/0009-2509(81)85117-2

Sporleder, F., Borka, Z., Solsvik, J., Jakobsen, H.A., 2012. On the population balance equation. Rev. Chem. Eng. 28. doi:10.1515/revce-2011-0013

Stoots, C.M., Calabrese, R. V, 1995. Mean velocity field relative to a Rushton turbine blade. AIChE J. 41, 1–11. doi:10.1002/aic.690410102

Valentas, K.J., Amundson, N.R., 1966. Breakage and Coalescence in Dispersed Phase Systems. Ind. Eng. Chem. Fundam. 5, 533–542. doi:10.1021/i160020a018

Villwock, J., Gebauer, F., Kamp, J., Bart, H.-J., Kraume, M., 2014a. Systematic Analysis of Single Droplet Coalescence. Chem. Eng. Technol. 37, 1103–1111. doi:10.1002/ceat.201400180

Villwock, J., Kamp, J., Kraume, M., 2014b. Systematic Analysis of Coalescence in Liquid/Liquid Dispersions, in: Kraume, M., Wehinger, G. (Eds.), Conference Proceedings of the 20th International Conference of Process Engineering and Chemical Plant Design. pp. 119–126.

Wegener, M., Grünig, J., Stüber, J., Paschedag, A.R., Kraume, M., 2007. Transient rise velocity and mass transfer of a single drop with interfacial instabilities - experimental investigations. Chem. Eng. Sci. 62, 2967–2978. doi:10.1016/j.ces.2007.03.003

Wegener, M., Kraume, M., Paschedag, A.R., 2010. Terminal and transient drop rise velocity of single toluene droplets in water. AIChE J. 56, 2–10. doi:10.1002/aic.11969

Wegener, M., Paul, N., Kraume, M., 2014. Fluid dynamics and mass transfer at single droplets in liquid/liquid systems. Int. J. Heat Mass Transf. 71, 475–495. doi:10.1016/j.ijheatmasstransfer.2013.12.024

Wu, H., Patterson, G.K., 1989. Laser-Doppler measurements of turbulent-flow parameters in a stirred mixer. Chem. Eng. Sci. 44, 2207–2221. doi:10.1016/0009-2509(89)85155-3

Wulkow, M., Gerstlauer, A., Nieken, U., 2001. Modeling and simulation of crystallization processes using parsival. Chem. Eng. Sci. 56, 2575–2588. doi:10.1016/S0009-2509(00)00432-2